Journal of Medicinal Chemistry

pubs.acs.org/jmc

Article

Stereochemistry-Driven Interactions of α,γ-Peptide Ligands with the Neuropeptide Y Y_4-Receptor

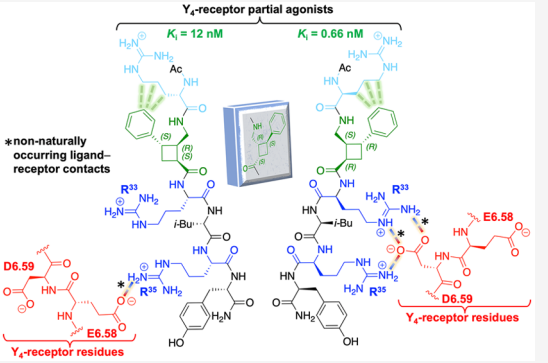
Eva Plut, Jacqueline C. Calderón, Vesna Stanojlović, Albert O. Gattor, Carina Höring, Laura J. Humphrys, Adam Konieczny, Sabine Kerres, Mario Schubert, Max Keller,* Chiara Cabrele,* Timothy Clark,* and Oliver Reiser*

Cite This: J. Med. Chem. 2023, 66, 9642−9657

Read Online

ACCESS | Metrics & More | Article Recommendations | Supporting Information

ABSTRACT: The G-protein-coupled Y_4-receptor (Y_4R) and its endogenous ligand, pancreatic polypeptide (PP), suppress appetite in response to food intake and, thus, are attractive drug targets for body-weight control. The C-terminus of human PP (hPP), T^{32}-R^{33}-P^{34}-R^{35}-Y^{36}-NH_2, penetrates deep into the binding pocket with its tyrosine-amide and di-arginine motif. Here, we present two C-terminally amidated α,γ-hexapeptides (**1a**/**b**) with sequence *Ac*-R^{31}-γ-CBAA^{32}-R^{33}-L^{34}-R^{35}-Y^{36}-NH_2, where γ-CBAA is the (1*R*,2*S*,3*R*)-configured 2-(aminomethyl)-3-phenylcyclobutanecarboxyl moiety (**1a**) or its mirror image (**1b**). Both peptides bind the Y_4R (K_i of **1a**/**b**: 0.66/12 nM) and act as partial agonists (intrinsic activity of **1a**/**b**: 50/39%). Their induced-fit binding poses in the Y_4R pocket are unique and build ligand−receptor contacts distinct from those of the C-terminus of the endogenous ligand hPP. We conclude that energetically favorable interactions, although they do not match those of the native ligand hPP, still guarantee high binding affinity (with **1a** rivaling hPP) but not the maximum receptor activation.



INTRODUCTION

Pancreatic polypeptide (PP) is a member of the neuropeptide (NPY) family that, in addition to PP and NPY, also includes peptide YY (PYY).[1,2] These three 36-residue C-terminally amidated peptides are agonists of the four G-protein-coupled Y_n receptors (Y_nR, n = 1, 2, 4, 5), although with different preferences: NPY and PYY bind the Y_1R, Y_2R, Y_5R, and, to a lesser extent, Y_4R, while PP binds the Y_4R and, to a lesser extent, Y_5R.[1,3−5] The Y_nR-mediated biological activities of PP, NPY, and PYY are manifold, covering the regulation of food intake, the release of neurotransmitters, and the control of cardiac and gastrointestinal functions.[1,6] Moreover, this multiligand−multi-receptor system plays a role in diseases like cancer,[7−9] obesity,[10,11] neurodegenerative[12] and cardiovascular[13] diseases, stress,[14−18] and mood disorders.[19−21] Given their implication for human health, many efforts have been made to develop molecules capable of selectively activating or blocking the Y_nR subtypes.[4,5,22−50]

Recently, the cryo-EM structures of porcine NPY (pNPY) bound to the Y_1R and Y_2R, and of human PP (hPP) bound to the Y_4R have been solved.[51] This represents a remarkable milestone in the four decades of research since PP and NPY were isolated for the first time from chicken pancreas[52] and porcine brain.[53] Indeed, the binding poses of hPP and pNPY in the respective ternary complex (ligand-Y_nR-G_{i1}) highlight the structural prerequisites of the ligand to obtain high affinity and selectivity for the receptor subtype, as well as its activation. In particular, the C-terminally amidated pentapeptide 32−36 of hPP and pNPY is crucial for all three aspects mentioned above, as it is the part of the ligand that penetrates deep into the binding pocket, forming both an energetically and functionally favorable network of polar and hydrophobic interactions. Most significant are the interactions of the C-terminal amide and the di-arginine motif R^{33}-X-R^{35}, which are shared by all members of the NPY family.[51] As for the C-terminal amide, this is H-bonded to the same Y_nR residues in all three receptor subtypes, which are threonine at position 61 of the transmembrane (TM) helix II (T2.61), Q3.32, and H7.39 (Figure 1A). In contrast, the di-arginine motif displays an interaction network that is unique for each receptor subtype: in the Y_2R, both R^{33} and R^{35} are salt-bridged with D6.59, and, additionally, R^{35} is salt-bridged with E^{205} from the extracellular loop 2, whereas only R^{35} is salt-bridged with D6.59 in the Y_1R and Y_4R, while R^{33} is H-bonded to N6.55. However, due to the presence of an additional acidic

Received: February 28, 2023
Published: July 13, 2023



Downloaded from pubs.acs.org/jmcmar/article-pdf/66/14/9642/4587513/jm3c00363.pdf by FREIE UNIV BERLIN user on 14 November 2026

ACS Publications

© 2023 The Authors. Published by American Chemical Society

https://doi.org/10.1021/acs.jmedchem.3c00363
J. Med. Chem. 2023, 66, 9642−9657

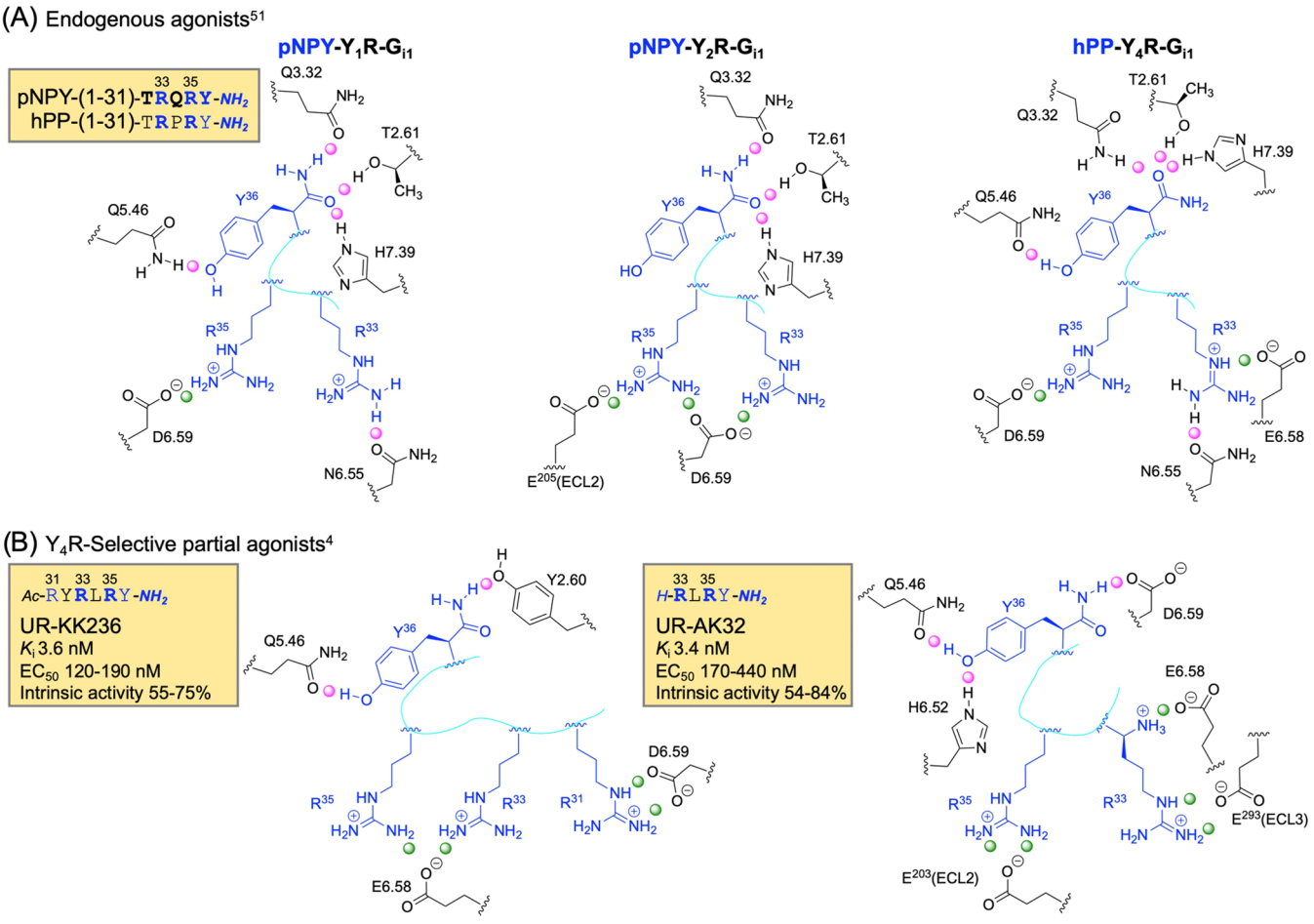


Figure 1. Ligand−receptor interactions of the conserved NPY/PP di-arginine motif R^{33}-X-R^{35} and the C-terminal amide. (A) Electrostatic contacts (H-bonds ◯, and salt bridges ◯) of the di-arginine motif and C-terminal tyrosine-amide of pNPY and hPP bound to the human $Y_{1,2}R$ and Y_4R, respectively, as found in the cryo-EM structures reported recently (PDB-ID: 7X9A, 7X9B, and 7X9C).[51] For the complete view of the ligand−receptor interactions, see ref 51. The sequence 32−36 of pNPY and hPP is reported in the box: the positions conserved across all species for each peptide are in bold.[1] (B) Electrostatic contacts of the Y_4R-selective partial agonists UR-KK236 and UR-AK32 containing the conserved NPY/PP di-arginine motif and C-terminal amide, as generated by induced-fit docking into a Y_4R homology model and reported recently[4] (for the complete view of the ligand−receptor interactions, see ref 4).

residue in the Y_4R, E6.58 (otherwise phenylalanine in the Y_1R and valine in the Y_2R), R^{33} forms a second ionic interaction.

In summary, a salt bridge between R^{35} and D6.59 allows the anchoring of the di-arginine motif into the binding pocket of all three Y_nR subtypes, while a second salt bridge between R^{33} and E6.58 is a feature only of the Y_4R subtype.

Short linear α-peptides displaying the C-terminally amidated, di-arginine motif of NPY/PP have been developed, which, despite their small size (four to eight residues), bind the Y_4R with high affinity but act as partial agonists, indicating that they are unable to induce maximum receptor activation.[4] Two examples are the partial agonists UR-KK236 and UR-AK32, whose sequences are reported in Figure 1B: by analyzing the results of their induced-fit docking into a Y_4R homology model based on the crystal structure of a κ-opioid receptor,[4] we noticed that the network of interactions between the di-arginine motif of the ligand and the two Y_4R acidic residues E6.58 and D6.59 differs significantly from that found in the cryo-EM structure of the endogenous ligand hPP in the Y_4R binding pocket.[51] Moreover, the C-terminal amide group of UR-KK236 and UR-AK32 does not interact with any of the three Y_4R polar side chains of T2.61, Q3.32, and H7.39, as done by hPP (Figure 1A), but instead with the side chain of Y2.60 and D6.59, respectively (Figure 1B).

In the present work, we evaluated how the type of ligand−receptor contacts involving the NPY/PP di-arginine motif and the C-terminal amide could influence the Y_4R binding and agonism of small peptides based on the hPP segment 32−36. For this, we developed a mixed α,γ-peptide analogue (**1**) of the Y_4R-selective partial agonist UR-KK236 and investigated its biological properties and induced-fit binding poses. We envisaged modifying the neighboring positions of the conserved NPY/PP di-arginine motif by the incorporation of mirror images of a bulky and conformationally constrained γ-residue to assess the effect of the geometric placement of the two basic side chains and the C-terminal end on receptor binding and activity (Scheme 1). We show that we could, indeed, obtain different ligand−receptor interaction networks for each stereoisomeric α,γ-peptide (**1a**/**b**), which, however, were distinct from those found in the ternary complex hPP-Y_4R-G_{i1},[51] but nevertheless resulting in low-nanomolar or even subnanomolar binding rivaling the natural ligand. Along with this, we observed only partial receptor activation, whereas the binding affinity could benefit from the energetically favorable interaction network of the di-arginine motif with the Y_4R.

https://doi.org/10.1021/acs.jmedchem.3c00363
J. Med. Chem. 2023, 66, 9642−9657

Downloaded from pubs.acs.org/jmcmar/article-pdf/66/14/9642/4587513/jm3c00363.pdf by FREIE UNIV BERLIN user on 14 November 2026

Scheme 1. α,γ-Peptide Analogues of the Y_4R-Selective Partial Agonist UR-KK236

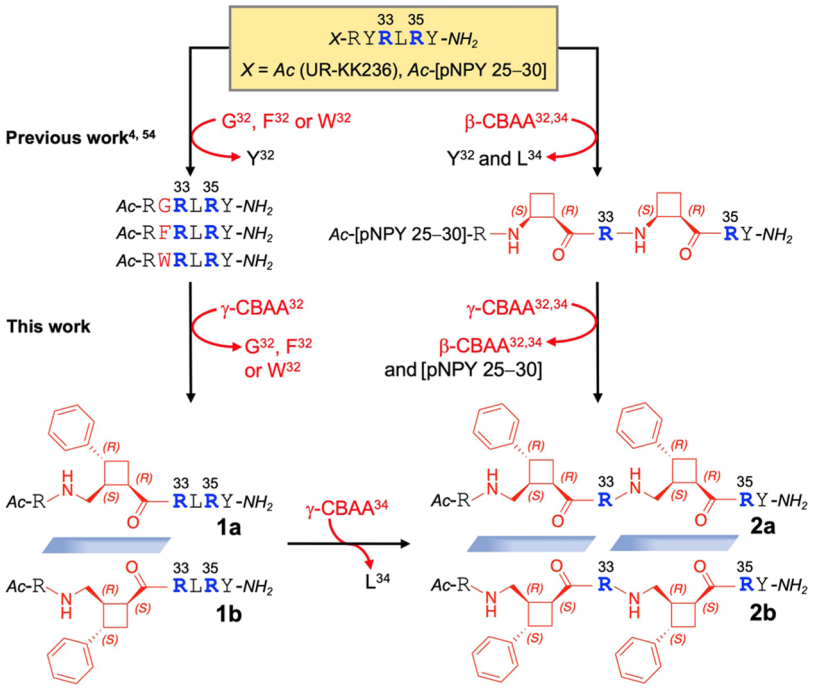


Table 1. Binding Affinity and Agonistic Potency of the α,γ-Peptide Analogues of UR-KK236 at the Y_nR Subtypes, and Comparison with the Endogenous Agonists hPP and pNPY, as well as with the Y_4R-Selective Partial Agonist UR-KK236 (n.d., not determined)

	hY_1R	hY_2R	hY_4R			hY_5R
peptide ligand	$pK_i \pm SEM/K_i$ (nM)[a]	$pK_i \pm SEM/K_i$ (nM)[b]	$pK_i \pm SEM/K_i$ (nM)[c]	$pEC_{50} \pm SEM/EC_{50}$ (nM)[d]	$\alpha \pm SEM$[d]	$pK_i \pm SEM/K_i$ (nM)[e]
hPP	6.35/440 ± 74[f]	<5.3/>5000[f]	9.16 ± 0.03/0.69[g]	8.94 ± 0.13/1.4	1.0	7.75/17 ± 1.5[f]
pNPY	9.42 ± 0.06/0.39[g]	9.31 ± 0.02/0.50[g]	7.92 ± 0.02/12	n.d.	n.d.	8.78 ± 0.08/1.7[g]
UR-KK236	5.93/1180 ± 380[h]	<5.3/>5000[h]	8.47/3.4 ± 1.3[h]	6.98 ± 0.14/110	0.58 ± 0.04	<5.3/>5000[h]
1a	6.64 ± 0.06/230[i]	<6.0/>1000	9.19 ± 0.04/0.66	7.73 ± 0.13/20	0.50 ± 0.03	<5.5/>3000
1b	<5.5/>3000	<5.5/>3000	7.93 ± 0.09/12	6.33 ± 0.25/610	0.39 ± 0.02	<5.5/>3000
2a	<6.0/>1000	<5.5/>3000	6.48 ± 0.07/340	n.d.	n.d.	<6.0/>1000
2b	<6.0/>1000	<5.5/>3000	6.05 ± 0.07/910	n.d.	n.d.	<6.0/>1000

[a]Determined by competition binding with [^{3}H]UR-MK299 (K_d = 0.044 nM,[33] c = 0.15 nM) at hY_1R-expressing SK-N-MC neuroblastoma cells. [b]Determined by competition binding with [^{3}H]propionyl-pNPY (K_d = 0.14 nM,[4] c = 0.5 nM) at CHO-hY_2R cells. [c]Determined by competition binding with [^{3}H]UR-KK200 (K_d = 0.67 nM,[35] c = 1 nM) at CHO-hY_4R-G_{qi5}-mtAEQ cells. [d]Agonistic potency (pEC_{50}, EC_{50}) and intrinsic activity α (relative to the effect of 1 μM hPP, α = 1) determined in a mini-G_{si} protein recruitment assay performed at HEK293T-NlucN-mG_{si}/Y_4R-NlucC cells.[56] [e]Determined by competition binding with [^{3}H]propionyl-pNPY (K_d = 11 nM,[57] c = 5 nM) at HEC-1B-hY_5R cells. (a–c, e) The structures of the tritiated compounds are shown in Figure S3. (a–e) Data represent mean values from three independent experiments performed in triplicate. [f]Reported by Berlicki et al.[54] Reported K_i values were converted to pK_i values. [g]Reported by Konieczny et al.[5] [h]Reported by Kuhn et al.[36] Reported K_i values were converted to pK_i values. [i]The competition binding curve is shown in Figure S4.

RESULTS AND DISCUSSION

Design of α,γ-Peptide Analogues of the Y_4R-Selective Partial Agonist UR-KK236. We performed amino-acid substitutions in the Y_4R-selective partial agonist UR-KK236, with the aim of obtaining analogues that can bind the Y_4R but whose structural characteristics require binding poses different from those of UR-KK236. Although previous work indicates Y^{32} and L^{34} to be particularly suited for N-terminally truncated PP and NPY analogues preferring the Y_4R over the other receptor subtypes,[4,24,36,39] we decided to modify the α-amino-acid sequence of the C-terminally amidated hexapeptide UR-KK236 at these two positions, as both showed good tolerance toward non-conservative substitutions (Scheme 1). For example, Y^{32} could be replaced with other aromatic residues, such as tryptophan and phenylalanine, or with glycine, without significant loss of Y_4R binding affinity.[4] Concerning the double substitution at positions 32 and 34, besides hydrophobic α-amino acids, conformationally constrained β-amino acids derived from cyclobutane (β-CBAA) and cyclopentane (β-CPAA), like the *cis*-configured (1*R*,2*S*)-2-amino-cyclobutane or cyclopentane carboxylic acids, could also be incorporated.[54] Because hydrophobic moieties are preferred, and a geometry-controlled expansion of the peptide backbone is, in principle, possible, we chose our recently developed γ-amino acid 2-(aminomethyl)-3-phenyl-cyclobutanecarboxylic acid (γ-CBAA),[55] whose inherent structural features include both hydrophobicity (i.e., phenyl-cyclobutyl moiety) and residue-directed peptide-backbone expansion along with partial rigidification (i.e., the cyclobutyl ring with the *cis*-configuration of the α-carboxyl and γ-aminomethyl substituents, in analogy with the well-tolerated β-CBAA used in a previous work[54]). Moreover, using the mirror images of the γ-amino acid gives the

Downloaded from pubs.acs.org/jmcmar/article-pdf/66/14/9642/4587513/jm3c00363.pdf by FREIE UNIV BERLIN user on 14 November 2026

https://doi.org/10.1021/acs.jmedchem.3c00363
J. Med. Chem. 2023, 66, 9642–9657

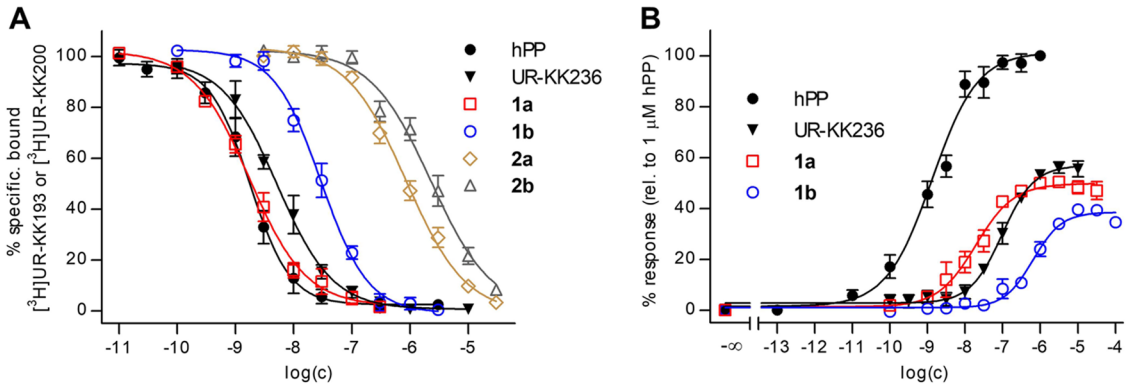


Figure 2. Y_4R binding and activation by the α,γ-peptide analogues of UR-KK236. (A) Binding curves of hPP, UR-KK236, **1a**, **1b**, **2a**, and **2b**, obtained from competition binding experiments with the Y_4R radioligand [^{3}H]UR-KK193 (K_d = 0.67 nM,[35] c = 0.6 nM) (UR-KK236) or [^{3}H]UR-KK200 (K_d = 0.67 nM,[35] c = 1 nM) (hPP, **1a**, **1b**, **2a**, **2b**) performed at intact CHO-hY_4R-G_{qi5}-mtAEQ cells. The structures of the tritiated compounds are shown in Figure S3. Data of hPP and UR-KK236 were taken from Konieczny et al.[5] and Kuhn et al.,[36] respectively. (B) Concentration−response curves of hPP, UR-KK236, **1a**, and **1b**, obtained from a hY_4R mini-G_{si} protein recruitment assay performed with HEK293T-NlucN-mG_{si}/Y_4R-NlucC cells.[56] (A, B) Data represent mean values ± standard error of the mean (SEM) from three independent experiments performed in triplicate. For K_i and EC_{50} values, see Table 1.

opportunity to modify the backbone sterically without changing the side-chain functionality. Thus, following the amino-acid substitution pattern applied in previous work,[4,54] we designed the α,γ-peptides **1** and **2** containing γ-CBAA at position 32 or both positions 32 and 34, respectively (Scheme 1). The α,γ-peptides were assembled by solid-phase peptide synthesis (SPPS) from N^{α}-fluorenylmethyloxycarbonyl(Fmoc)-protected α-amino acids and N^{γ}-Fmoc-protected γ-amino acids, which were then purified by reverse-phase high-performance liquid chromatography (RP-HPLC) to reach purities of at least 95% (Figures S1 and S2).

Stereoisomeric α,γ-Peptides 1a and 1b Bind the Y_4R with Different Affinities and Act as Partial Agonists. To evaluate the impact of the incorporation of (1*R*,2*S*,3*R*)-γ-CBAA and its enantiomer at positions 32 and 34 of UR-KK236 on Y_nR binding, we performed a radioligand competition binding assay on the following cell lines: Y_1R-expressing SK-N-MC, CHO-hY_2R, CHO-hY_4R-G_{qi5}-mtAEQ, and HEC-1B-hY_5R (Table 1 and Figure 2A). The replacement of Y^{32} with (1*S*,2*R*,3*S*)-γ-CBAA was well tolerated, resulting in only a threefold lower affinity of the α,γ-peptide **1b** for Y_4R compared to UR-KK236 (K_i 12 nM vs 3.4 nM[36]). The enantiomer (1*R*,2*S*,3*R*)-γ-CBAA was tolerated even better: the α,γ-peptide **1a** binds to the Y_4R 18-times more strongly than **1b** (K_i 0.66 nm vs 12 nM), and as strongly as the native human ligand hPP (K_i 0.66 nm vs 0.69 nM[5]), which highlights the importance of the stereochemistry of the constrained γ-residue. In analogy with UR-KK236, both α,γ-peptides **1a** and **1b** exhibit very high Y_4R selectivity, with K_i (Y_1R/Y_4R) ratios of 350 and >250, respectively.

In contrast to **1a** and **1b**, the α,γ-peptides **2a** and **2b**, which contain (1*R*,2*S*,3*R*)-γ-CBAA or (1*S*,2*R*,3*S*)-γ-CBAA at both positions 32 and 34, displayed only submicromolar Y_4R binding affinity, with K_i values of 340 and 910 nM, respectively. We attribute the lack of binding after the replacement of L^{34} with γ-CBAA mainly to the bulkiness of the unnatural γ-residue, in accordance with the recently reported data[4] on an analogue of UR-KK236 containing tryptophan instead of leucine at position 34, which show moderate Y_4R binding affinity (K_i 97 nM) and, moreover, no receptor activation. Therefore, hydrophobicity and steric hindrance play an important role at position 34 and need to be balanced to retain strong Y_4R binding and activity. In light of this, we desisted from preparing mono-substituted γ-CBAA[34]-containing analogues of UR-KK236.

Next, we assessed the functional activity of the strong Y_4R ligands **1a** and **1b** by using a recently reported mini-G_{si} protein recruitment assay[56] (Table 1 and Figure 2B). Both α,γ-peptide ligands act as partial agonists, inducing 40−50% receptor activation compared to that induced by hPP. However, the stronger ligand **1a** is also a more potent partial agonist, displaying an EC_{50} value of 20 nM against the 30-fold higher value (610 nM) of **1b**.

Stereoisomeric α,γ-Peptides 1a and 1b Show Different Susceptibilities toward the Metalloprotease Angiotensin-Converting Enzyme (ACE). The stability of the γ-CBAA-containing peptides **1a** and **1b** in human plasma was investigated and compared to that of the α-peptide ligand UR-KK236. The time-dependent loss of intact peptide was monitored using the recovery ratios between peptide and internal standard (1-methyl-D-tryptophan) at increasing incubation times (Figure 3 and Tables S1 and S2). Based on the extrapolated rate constants, **1a** degraded six times faster than its stereoisomer **1b** and more than three times faster than UR-KK236.

Recently, we identified the dipeptidyl carboxypeptidase ACE as the protease responsible for the degradation of analogues of UR-KK236 in plasma by cleaving the peptide bond between L^{34} and R^{35}.[5] Thus, we incubated the γ-CBAA-containing peptides **1a** and **1b** in human plasma in the presence of ramipril, which is a selective ACE inhibitor. The α,γ-peptides remained intact over four hours of incubation at 37 °C (Figure S5), confirming that they are also ACE substrates. However, the fact that **1a** is degraded faster than UR-KK236 and **1b** indicates that the three peptides have different ACE susceptibilities: since, in general, the structural stability of peptides and proteins inversely correlates with their susceptibility to proteolysis,[58] we hypothesize that the six times faster cleavage of the bond L^{34}−R^{35} in **1a** is related to higher flexibility and, consequently, to a quick adaptation of the substrate to the active site of the protease. Yet, we cannot exclude that, besides different conformational preferences, the steric fit of the residue at position 32 might also affect the adaptation of the three peptides to the active site of ACE positively or negatively.[58]

Despite the perceptible, although weak, effect of γ-CBAA[32] on the proteolytic susceptibility of the dipeptide L^{34}−R^{35}, a

Downloaded from pubs.acs.org/jmcmar/article-pdf/66/14/9642/4587513/jm3c00363.pdf by FREIE UNIV BERLIN user on 14 November 2026

https://doi.org/10.1021/acs.jmedchem.3c00363
J. Med. Chem. 2023, 66, 9642−9657

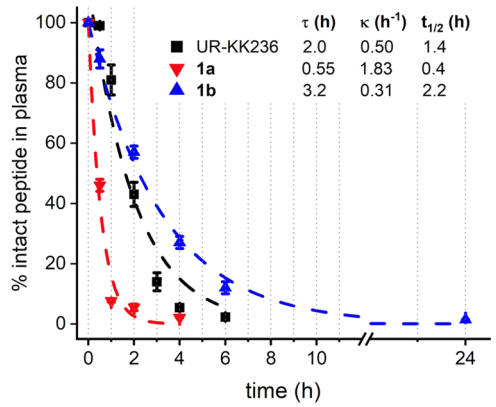


Figure 3. Degradation rates of the α,γ-peptide analogues of UR-KK236 in human blood plasma. Time-dependent loss of intact peptide (from an initial concentration of 100 μM) in plasma/PBS (1:2 v/v). The data points represent mean values ± SEM from three independent experiments and were fitted by nonlinear regression (monoexponential decay, Figures S6–S8) to extrapolate the time constants (τ), rate constants (κ), and half-life times ($t_{1/2}$).

substantial chemical modification of the latter will be necessary to avoid ACE-mediated hydrolysis. Based on our previous data about the tolerance of β-CBAA and β-CPAA at position 34 (Scheme 1),[54] we believe that α,β,γ-analogues of the partial α,γ-peptide agonists **1a** and **1b** are promising future candidates to gain stability against ACE.

Stereoisomeric α,γ-Peptides 1a and 1b Adopt Distinct Locally Ordered Structures in a Polar Environment. Short amino-acid sequences generally possess inherent flexibility; however, the formation of locally ordered structures can occur through short-to-medium-range interactions, like those formed in the initial stages of the folding of larger peptides and proteins.[59−61] We investigated the conformational properties of **1a** and **1b** by circular dichroism (CD) and 2D-NMR spectroscopy. The CD spectra of the two stereoisomeric α,γ-peptides in phosphate buffer are almost mirrored (Figure 4A): this suggests that the major contributions to the CD signals of **1a** and **1b** derive from (1*R*,2*S*,3*R*)-γ-CBAA and its enantiomer, respectively. A minor contribution from the flanking α-amino-acid residues at 195−208 and 220−235 nm is visible, as evidenced by the superposition of the CD curve of **1b** and the mirrored CD curve of **1a** (the lack of overlap between the two CD curves is highlighted by the hatched area and is alternatively represented by the corresponding difference CD spectrum in the inset of Figure 4A). Conversely, in the presence of a secondary-structure stabilizing solvent such as 2,2,2-trifluoroethanol (TFE),[62−66] **1a** and **1b** show CD spectra that are no longer specular, revealing substantially different intrinsic structural propensities dictated by the configuration of the γ-amino-acid residue and the organic solvent (Figure 4B). Interestingly, the CD spectrum of **1a** is much more intense than that of **1b**, which indicates that the TFE-stabilized conformation of **1a** is better defined than that of **1b**; however, since the reference CD spectra for the secondary structures of polypeptides based on the proteinogenic α-amino acids are not applicable for the interpretation of CD spectra of mixed α,γ-peptides, one should refrain from making assumptions about the type of the secondary structure adopted by **1a** and **1b** in 30% TFE.

The CD spectra of the α,γ-peptides **2a** and **2b**, which contain γ-CBAA at positions 32 and 34, maintain the same shape both in the absence and presence of TFE, while the intensity of the CD signal changes slightly (**2b**) or moderately (**2a**). This indicates that TFE does not induce a conformational transition but, rather, further stabilizes the structure already partially formed (Figure 4C).[67,68] Therefore, the two higher γ-substituted analogues of UR-KK236, especially **2b**, display a more rigid and, consequently, less environment-dependent structure.

To search for local structures in the α,γ-peptides **1a**, **1b**, **2a**, and **2b**, whose presence would explain the different degrees of conformational flexibility suggested by the results of the enzymatic degradation and the CD measurements, we recorded NMR spectra in water and used both the chemical shifts and the NOE cross-peaks to characterize the structural properties of the peptides. NOE-constrained structure calculations delivered an ensemble of low-energy conformations for each peptide, as shown in Figure 5. The two nanomolar Y_4R ligands **1a** and **1b** display a well-defined conformation of the α,γ-dipeptide R^{31}-γ-$CBAA^{32}$, with the side chain of R^{31} and the phenyl ring of γ-$CBAA^{32}$ being in close proximity (Figure 5A,B). Such compact side-chain arrangement is supported not only by the NOE cross-peaks (Table S11) but also by the increasing up-field shift of the NMR resonances from the H^{ε} to the H^{β} protons of R^{31} with respect to the corresponding random-coil chemical shifts,[69] which reflects a ring-current effect of the phenyl group especially

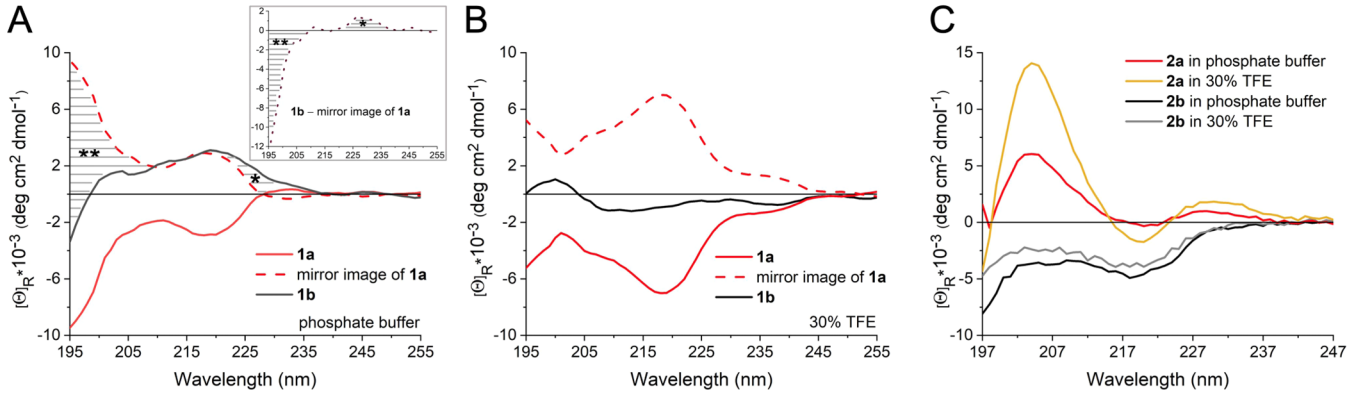


Figure 4. CD spectra of the α,γ-peptide analogues of UR-KK236. (A) CD curves of **1a** and **1b** in phosphate buffer (50 mM, pH 7.3). The hatched area highlights the lack of overlap between the CD curve of **1b** and the mirrored CD curve of **1a**, especially at 195−208 nm (**) and 220−235 nm (*), as shown also in the inset. (B) CD curves of **1a** and **1b** in phosphate buffer (50 mM, pH 7.3) with 30% TFE. (C) CD curves of **2a** and **2b** in phosphate buffer (50 mM, pH 7.3) with and without 30% TFE.

Downloaded from pubs.acs.org/jmcmar/article-pdf/66/14/9642/4587513/jm3c00363.pdf by FREIE UNIV BERLIN user on 14 November 2026

https://doi.org/10.1021/acs.jmedchem.3c00363
J. Med. Chem. 2023, 66, 9642−9657

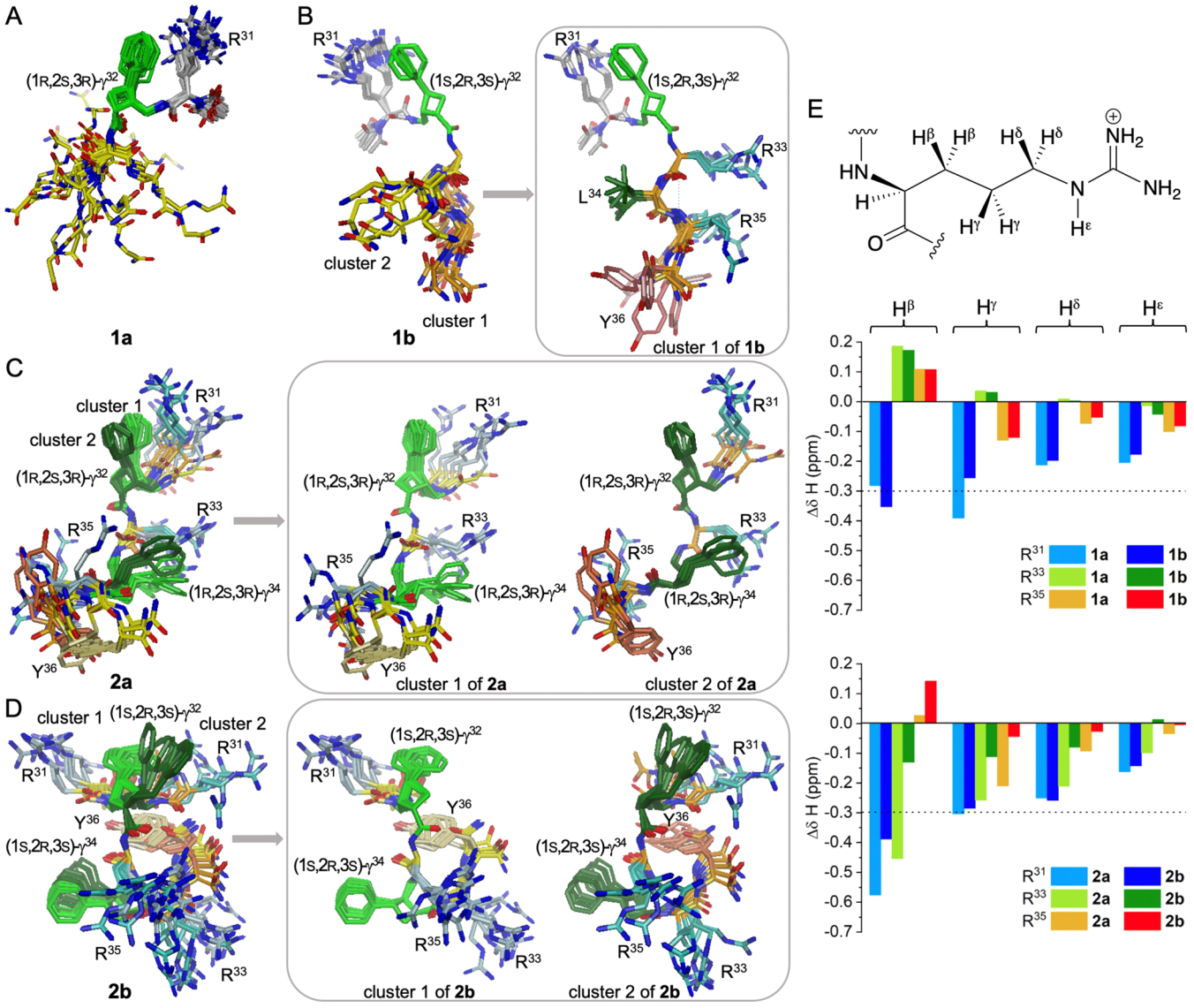


Figure 5. NMR solution structures of the α,γ-peptide analogues of UR-KK236. (A–D) Superposition of the low-energy structures of (A) **1a**, (B) **1b**, (C) **2a**, and (D) **2b**. (B–D) The identified clusters are shown separately in the gray frames: (B) cluster 1 displaying an inverse γ-turn at L^{34}, indicated with a dotted light-blue line; (C, D) clusters 1 and 2 (see also Figures S9 and S10 for further views). (E) Chemical shift deviations from random-coil values[69] of the arginine side-chain protons $H^{\beta\text{-}\varepsilon}$ in peptides **1a** and **1b** (upper graph), and **2a** and **2b** (bottom graph). The average of the experimental values for the two H^{γ} protons reported in Tables S3, S5, S7, and S9 was used to calculate $\Delta\delta$ H^{γ}.

on the methylene groups and suggests the presence of CH–π interactions (Figure 5E).

Unlike the rigid N-terminal α,γ-dipeptide 31–32, the C-terminal tetrapeptide 33–36 is conformationally less well-defined in both ligands but with significant differences, with ligand **1a** showing no preferred backbone orientation (Figure 5A) and **1b** displaying mainly two backbone orientations (clusters 1 and 2, Figure 5B). Interestingly, the more populated conformation (cluster 1 in the gray frame of Figure 5B) includes backbone conformations that exhibit an inverse γ-turn at L^{34}; this residue also exhibits a significant deviation of the amide-proton chemical shift from the random-coil value,[70] likely reflecting a stiffening of the backbone at position 34 (Figure S11A). The different degrees of flexibility of the C-terminal tetrapeptides of ligands **1a** and **1b** could explain their different stabilities in human blood plasma: indeed, the presence of a local structural element like a γ-turn could be sufficient to slow down the ACE-catalyzed cleavage of the peptide bond L^{34}–R^{35} in the ligand **1b**.

Further, we elucidated the NMR solution structures of the two submicromolar Y_4R α,γ-peptide ligands **2a** and **2b** (Figure 5C,D). As already suggested by their nearly TFE-independent CD spectra (Figure 4C), the two peptides adopt a better-defined backbone conformation than the nanomolar Y_4R ligands **1a** and **1b**. Also, **2b** adopts a more compact conformation than **2a**: a reversal of the backbone orientation occurs after position 34 (Figures 5D and S10D,E), which directs the phenol ring of Y^{36} to point back toward the N-terminal α,γ-dipeptide backbone 31–32. In fact, the backbone-amide proton of Y^{36} is shifted downfield by about 0.6 ppm with respect to the random-coil value,[70] suggesting substantial local structural effects (Figure S11B). Instead, in peptide **2a**, the C-terminal Y^{36}-amide points away from the N-terminus and maintains a certain degree of flexibility (Figures 5C and S9D). This might reflect the slightly better affinity of **2a** compared to **2b** (0.3 vs 0.9 μM, Table 1), as the side

https://doi.org/10.1021/acs.jmedchem.3c00363
J. Med. Chem. 2023, 66, 9642–9657

Downloaded from pubs.acs.org/jmcmar/article-pdf/66/14/9642/4587513/jm3c00363.pdf by FREIE UNIV BERLIN user on 14 November 2026

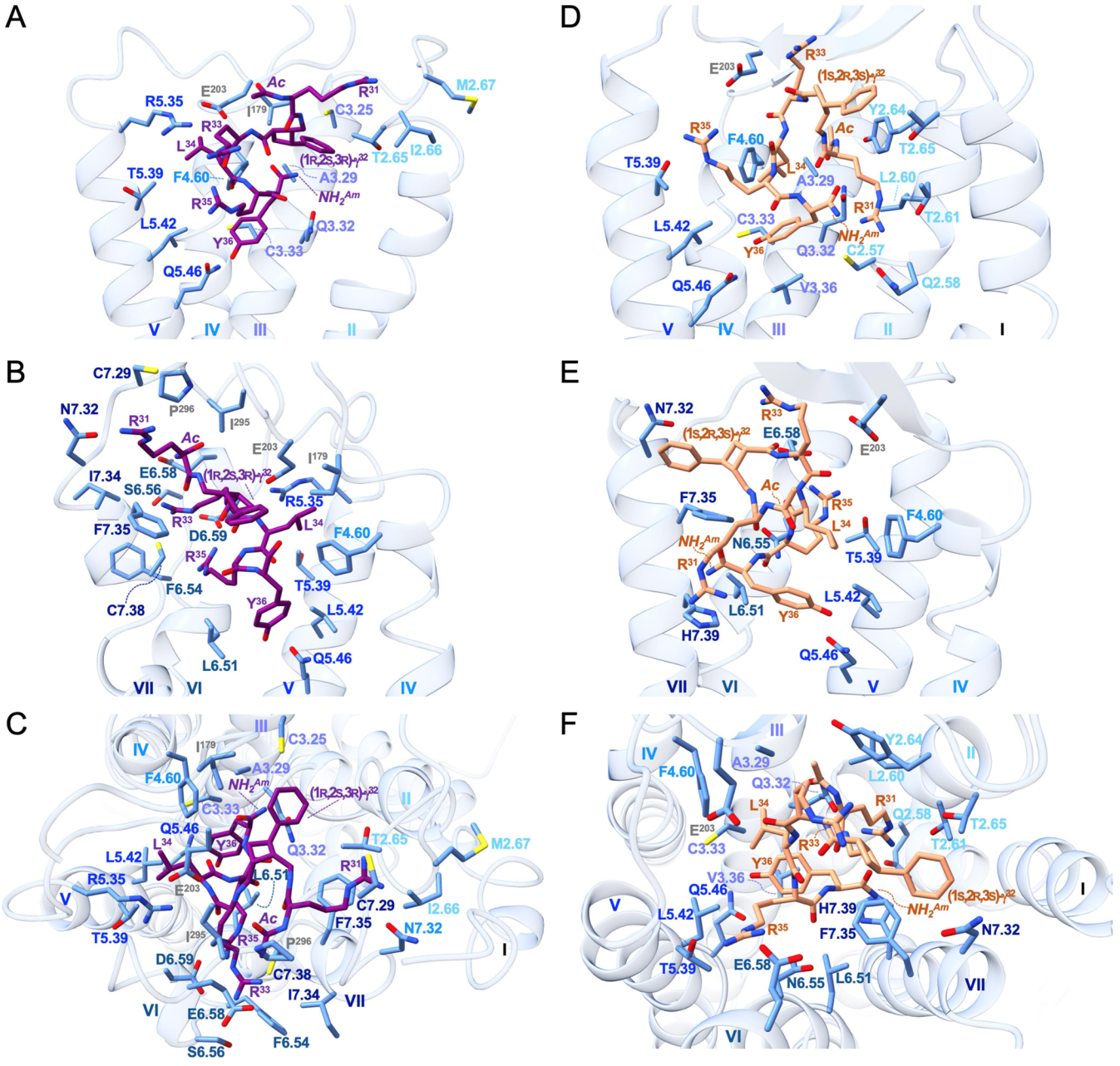


Figure 6. Induced-fit docking of the α,γ-peptides **1a** and **1b** into the human Y_4R model built based on the cryo-EM structure of the ternary complex hPP-Y_4R-G_{i1} (PDB-ID: 7X9C[51]). Docking pose of (A−C) **1a** and (D−F) **1b**. (A−F) The residues were displayed by setting a distance cut-off of 5 Å. The color code of the Y_4R-residue labels reflects their belonging to the TM helices II−VII (light to dark blue) and extracellular loops (gray). (A, B, D, E) Side view. (C, F) Top view. Carbon atoms of **1a**, **1b**, and the Y_4R side chains are in purple, salmon, and turquoise, respectively. Nitrogen, oxygen, and sulfur atoms are shown in blue, red, and yellow, respectively.

chain of Y^{36} and the C-terminal amide must be able to penetrate deeply into the binding pocket, as shown by both the endogenous Y_4R ligand hPP[51] and UR-KK236.[4]

Overall, the NMR analysis of the four α,γ-peptides shows that incorporating γ-CBAA into an α-amino-acid sequence can help stiffen the local backbone conformation: in fact, γ-CBAA is prone to undergo CH−π interactions with the methylene groups of the preceding side chain. When the (1*R*,2*S*,3*R*)-configuration is used, both R^{31}-γ-CBAA^{32} and R^{33}-γ-CBAA^{34} show CH−π interactions (**2a**), whereas only the N-terminal R^{31}-(1*S*,2*R*,3*S*)-γ-CBAA^{32} presents CH−π contacts (**2b**) (Figure 5E). Moreover, besides directly interacting with the preceding residue, γ-CBAA indirectly affects the conformation of the succeeding residues, as indicated by the different orientation adopted by the C-terminal α-dipeptide 35−36 in **2a** and **2b**, which leads to open and closed structures, respectively, depending on the stereochemistry of the γ-residue at position 34 (Figure 5C,D). Also, the C-terminal α-tetrapeptide 33−36 in **1a** and **1b**, which follows γ-CBAA^{32} in the (1*R*,2*S*,3*R*)- and (1*S*,2*R*,3*S*)-configurations, respectively, displays distinct conformational ensembles with different degrees of flexibility (Figure 5A,B); as mentioned above, this may contribute to modulating the susceptibility of the α-peptide backbone to proteolysis.

Stereoisomeric α,γ-Peptides 1a and 1b Build Distinct Induced-Fit Structures with Unique Ligand−Receptor Interaction Networks. After having shown that **1a** and **1b**

https://doi.org/10.1021/acs.jmedchem.3c00363
J. Med. Chem. 2023, 66, 9642−9657

Downloaded from pubs.acs.org/jmcmar/article-pdf/66/14/9642/4587513/jm3c00363.pdf by FREIE UNIV BERLIN user on 14 November 2026

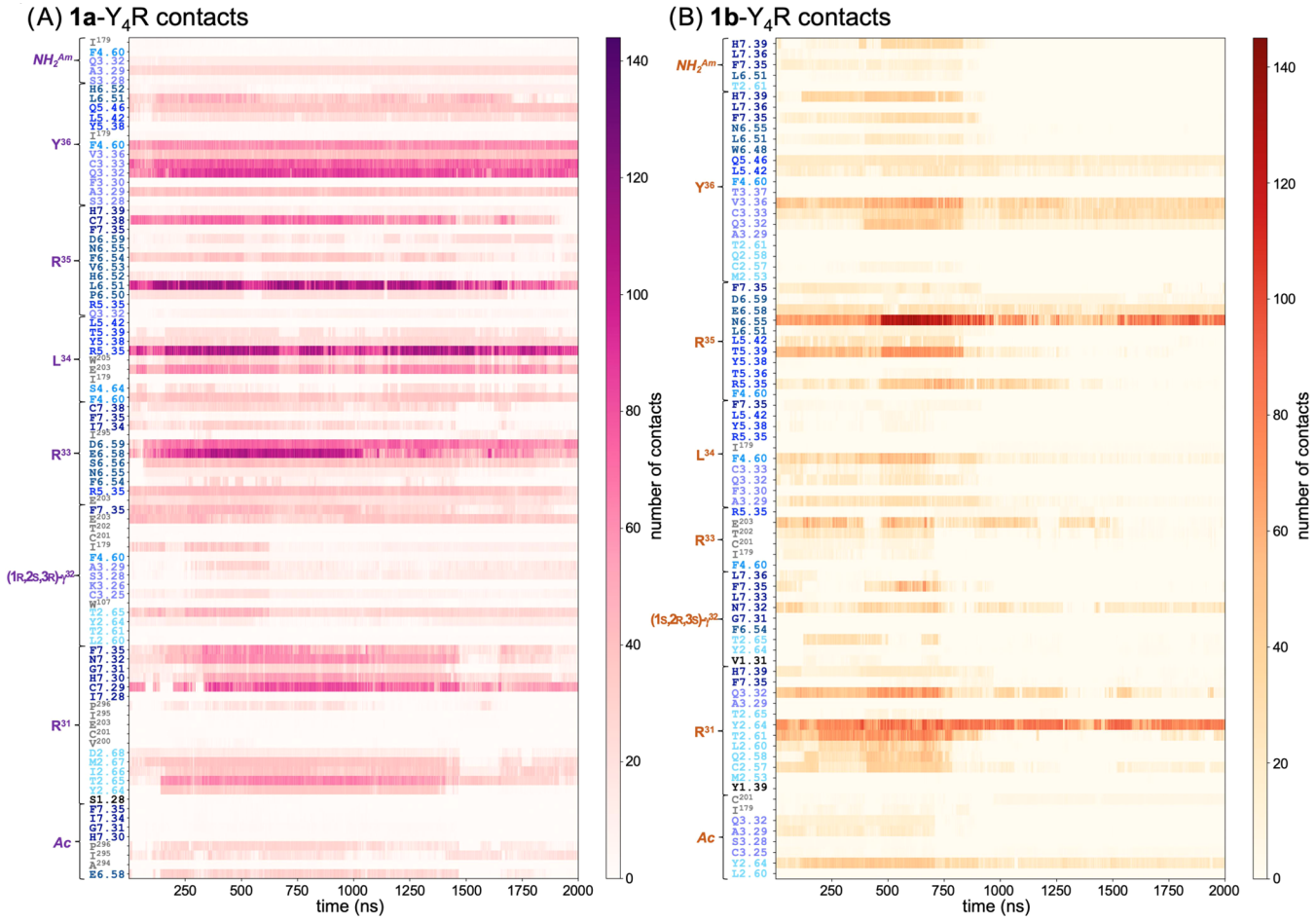


Figure 7. Number of contacts between the α,γ-peptides **1a** and **1b** and the human Y_4R model built based on the cryo-EM structure of the ternary complex hPP-Y_4R-G_{i1} (PDB-ID: 7X9C[51]) during MD simulation. (A) **1a**-Y_4R contacts during MD simulation (run 3). (B) **1b**-Y_4R contacts during MD simulation (run 2). (A, B) The color code of the residue labels for the ligand and Y_4R is the same as in Figure 6.

have different conformational preferences in the unbound state affecting their ACE-mediated degradation, we performed induced-fit docking and molecular dynamics (MD) simulations to gain insight into their receptor-bound structure. For this purpose, we built a Y_4R model based on the recently published cryo-EM structure of the ternary complex hPP-Y_4R-G_{i1} (PDB-ID: 7X9C[51]). The top-scored binding pose of each α,γ-peptide was selected for 2 μs of unconstrained MD simulations conducted in triplicate. Structural stability was analyzed by computing the root-mean-square deviation (RMSD) of the receptor and ligand peptide-backbone atoms with respect to the equilibrated starting structure, whereas root-mean-square fluctuations (RMSF) were calculated for all peptide atoms. Altogether, the three simulations conducted for **1a** and **1b** showed RMSD values from the equilibrated starting structure of 0.09 Å up to 3.9 Å during the production run, while the RMSD values for the Y_4R ranged from 0.29 to 5.8 Å (Figures S12 and S13). The two α,γ-peptides display remarkably different induced-fit structures (Figures 6 and S14): in the weaker ligand **1b**, the backbone adopts a bent conformation that places the N-terminal R^{31} and the C-terminal Y^{36}-amide in proximity, with 5.7 Å between the respective α-carbon atoms (Figure S14B). Such a closed conformation is stabilized by a bifurcated H-bond of the carbonyl oxygen of R^{31} with the α-amide protons of R^{35} and Y^{36}. Additional intramolecular interactions, which further stabilize the induced-fit structure of **1b**, are a backbone-to-side-chain H-bond between the carbonyl oxygen of γ-CBAA^{32} and the NH$^{\varepsilon}$ proton of R^{33}, and side chain-to-side chain CH$-\pi$ contacts between L^{34} and Y^{36}.

A very different induced-fit structure is shown by the stronger ligand **1a**, whose backbone conformation is akin to a β-bend ribbon (Figure S14A):[71] in detail, the N-terminal bend, which is larger than the standard ten-membered β-bend[71] because of the presence of the γ-residue, is characterized by a weak i $-$ i + 3 H-bond between the carbonyl oxygen of the N-terminal acetyl group and the α-amide proton of R^{33}, with 5.2 Å between the methyl carbon atom of the acetyl group and the α-carbon atom of R^{33}. It follows a distorted C-terminal β-bend stabilized by an i $-$ i + 3 H-bond between the carbonyl oxygen of γ-CBAA^{32} and the α-amide proton of R^{35}, with 5.4 Å between the respective α-carbon atoms. Additional intramolecular H-bonds contribute to the stabilization of the induced-fit structure of **1a**: in particular, a bifurcated H-bond of the carbonyl oxygen of R^{33} with both the α-amide proton and the guanidinium group of R^{35}, generating a distorted inverse γ-turn at L^{34}. Moreover, an i $-$ i + 2 backbone H-bond is formed between the carbonyl oxygen of L^{34} and the α-amide proton of Y^{36}, shaping an inverse γ-turn at R^{35}. Unlike **1b**, in which the C-terminal amide group is 4.4 Å from the side chain of the N-terminal R^{31}, the C-terminal amide group of **1a** is found to be 3.7 Å from the phenyl ring of γ-CBAA^{32}. Another remarkable difference between **1a** and **1b** is that the side chains of R^{33} and R^{35} in **1a** are similarly oriented and close to each

https://doi.org/10.1021/acs.jmedchem.3c00363
J. Med. Chem. 2023, 66, 9642−9657

Downloaded from pubs.acs.org/jmcmar/article-pdf/66/14/9642/4587513/jm3c00363.pdf by FREIE UNIV BERLIN user on 14 November 2026

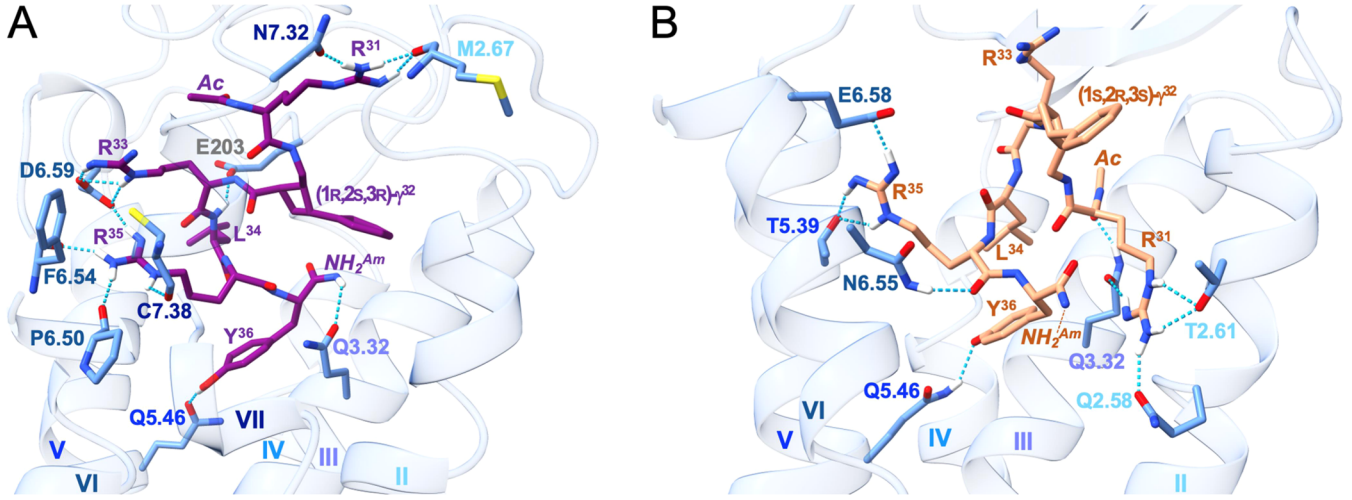


Figure 8. Electrostatic ligand−receptor networks of the α,γ-peptides **1a** and **1b**. H-bond and salt-bridge interactions between (A) **1a** or (B) **1b** and the human Y_4R model built based on the cryo-EM structure of the ternary complex hPP-Y_4R-G_{i1} (PDB-ID: 7X9C[51]). H-bonds were displayed by using default values of Chimera X[74,75] (distance tolerance of 0.4 Å and an angle tolerance of 20°). For the color code of atoms and labels, see the legend to Figure 6. For additional views, see Figure S22.

other, with about 5 Å between the two guanidinium groups, compared to about 10 Å in the case of **1b** (Figure S14).

Analysis of the ligand−receptor contacts and their energies during the MD simulations reveals that **1a** interacts with the binding pocket more strongly than **1b** (Figure 7). For example, during the MD simulations, the C-terminal Y^{36} shows frequent contacts with Q3.32$^{(121)}$, C3.33$^{(122)}$, and F4.60$^{(174)}$ in the case of **1a** (Figure 7A) but only with V3.36$^{(125)}$ in the case of **1b** (Figure 7B). Interestingly, the phenol hydroxyl group of Y^{36} is H-bonded to the side chain of Q5.46$^{(222)}$, acting as a H-bond acceptor in **1b** but as a donor in **1a** (Figure 8); the latter is analogous to the bound natural ligand hPP.[51] Importantly, the C-terminal amide serves as a H-bond donor to the side chain of Q3.32$^{(121)}$ in **1a** but not in **1b**, where it is instead the N-terminal acetyl group that forms a H-bond with Q3.32$^{(121)}$ (Figure 8). In the bound natural ligand hPP, the C-terminal amide is also H-bonded to Q3.32$^{(121)}$, however, acting as an acceptor.[51]

Remarkably different arrangements are observed for both R^{33} and R^{35} in the two induced-fit α,γ-peptides: while R^{33} in **1b** shows only a few transient contacts within the binding pocket (mainly with E^{203}, Figure 7B), but no H-bonds or salt bridges, R^{33} in **1a** not only interacts with E6.58$^{(288)}$, E^{203}, and R5.35$^{(211)}$ (Figure 7A) but it is also salt-bridged to D6.59$^{(289)}$ (Figures 8A and S19). The side chain of R^{35} in **1b** is salt-bridged and H-bonded to the side chains of E6.58$^{(288)}$ and T5.39$^{(215)}$, respectively (Figures 8B and S21), whereas its backbone carbonyl oxygen forms a H-bond with the side chain of N6.55$^{(285)}$ (Figure 8B). The network of interactions of R^{35} in **1a** is entirely different: in this case, the basic side chain is salt-bridged to D6.59$^{(289)}$ (Figure S20) and H-bonded to the backbone carbonyl oxygens of P6.50$^{(280)}$, F6.54$^{(284)}$, and C7.38$^{(307)}$ (Figure 8A). In the natural ligand hPP, R^{33} and R^{35} are involved in salt bridges with E6.58$^{(288)}$ and D6.59$^{(289)}$, respectively (Figure 1A),[51] which means that neither of the two induced-fit structures of **1a** and **1b** reproduces such native salt-bridge patterns faithfully, although **1a** is closer to mimicking them. Indeed, whereas R^{33} in **1b** is distant from E6.58$^{(288)}$, and R^{35} is salt-bridged to E6.58$^{(288)}$ rather than to D6.59$^{(289)}$, in the case of **1a**, R^{33} and R^{35} are both salt-bridged to D6.59$^{(289)}$, but R^{33} also makes many contacts with E6.58$^{(288)}$ during the MD simulation (Figure 7). In **1b**, L^{34} is barely involved in stable contacts within the binding pocket, whereas the same residue in **1a** interacts strongly with R5.35$^{(211)}$ and E^{203}, also forming a backbone-to-side chain H-bond with the latter (Figures 7A and 8A). The γ-residue γ-CBAA^{32} in **1b** shows a moderate number of transient contacts with residues from the TM helices II and VII, which include T2.65$^{(102)}$ and N7.32$^{(301)}$ (Figure 7B). For comparison, P^{34} in the natural ligand hPP is involved in hydrophobic packing against the TM helices II and VII, especially with the side chains of T2.61$^{(98)}$ and F7.35$^{(304)}$,[51] which suggests that the γ-residue at position 32 of **1b** partially occupies the site of hPP's P^{34}, albeit penetrating less deeply. In **1a**, the γ-residue makes contacts not only with the TM helices II and VII but also with the TM helix III (Figure 7A), which is likely to result in a slightly higher Van der Waals interaction energy for this bulky moiety in **1a** than in **1b** (Figures S16 and S18). Finally, the N-terminal R^{31} in **1b** interacts mainly with the TM helix II, forming side chain-to-side chain H-bonds with Q2.58$^{(95)}$ and T2.61$^{(98)}$ (Figure 8B), whereas, in the case of **1a**, it makes contacts with several residues from the TM helices II and VII, including M2.67$^{(104)}$ and N7.32$^{(301)}$ (Figure 8A).

Given the relevance of intermolecular salt bridges for ligand recognition in GPCRs,[48,72,73] it is not surprising that the di-arginine motif of **1a** and **1b** plays a prominent role in the interaction of the ligands with the Y_4R: especially the induced-fit structure of **1a**, which is also the stronger ligand, displays the more favorable electrostatic interactions for the di-arginine motif, as R^{33} and R^{35} are nearly equidistant from D6.59$^{(289)}$, forming a stable network of H-bonds and salt bridges between the three side chains. Thus, both the basic residues contribute to the electrostatic energy of the ligand−receptor complex. In contrast, in **1b**, only R^{35} is salt-bridged to E6.58$^{(288)}$, while R^{33} lacks stable polar interactions, as shown by MD simulations (Figure 7B). However, other energetic factors cannot be excluded: for example, the conformational transition of **1a** from the free to the bound state is likely to make a major contribution to the formation of a tight binding, since the induced-fit structure of **1a** shows a greater number of intramolecular contacts than that of **1b**, which, together with

Downloaded from pubs.acs.org/jmcmar/article-pdf/66/14/9642/4587513/jm3c00363.pdf by FREIE UNIV BERLIN user on 14 November 2026

https://doi.org/10.1021/acs.jmedchem.3c00363
J. Med. Chem. 2023, 66, 9642−9657

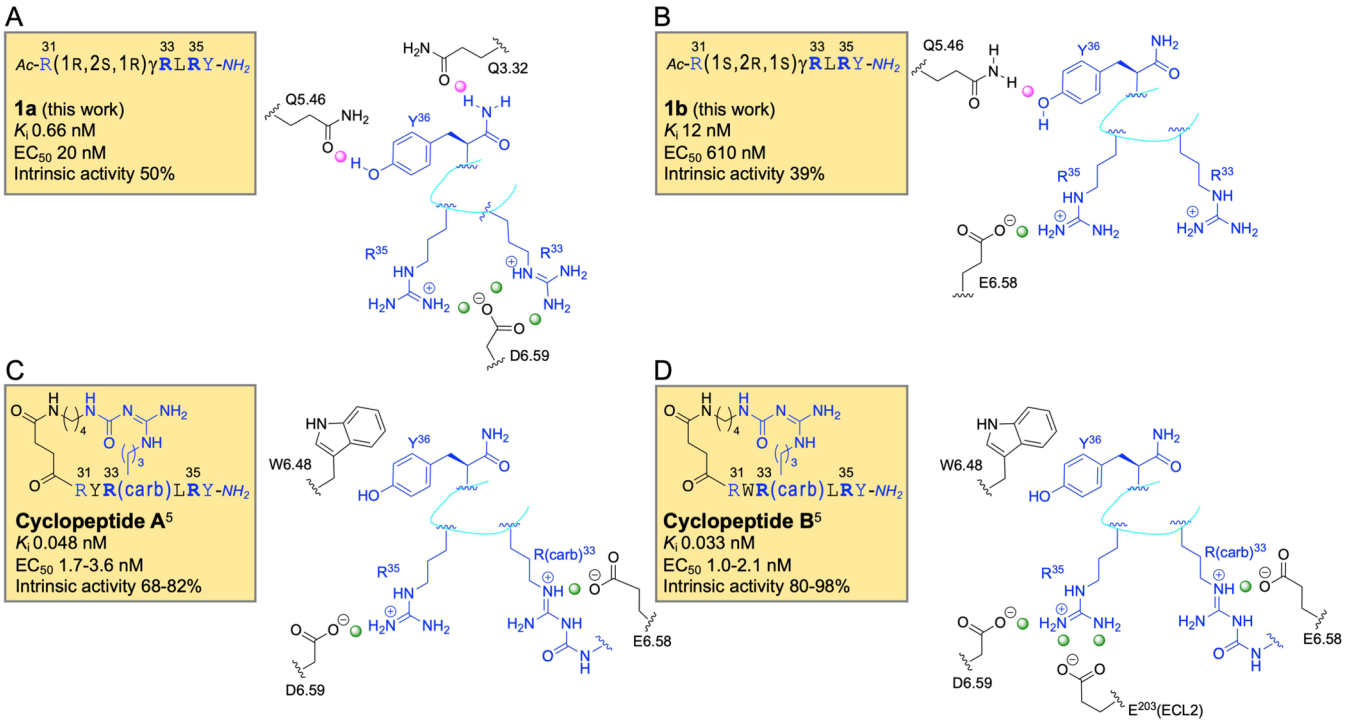


Figure 9. Ligand−receptor interactions of the di-arginine motif R^{33}-X-R^{35} and C-terminal Y^{36}-amide in the Y_4R partial agonists **1a** and **1b**, and comparison with two cyclic analogues of UR-KK236. (A, B) Electrostatic contacts (H-bonds ❍, and salt bridges ❍) of the di-arginine motif and C-terminal tyrosine-amide of the α,γ-peptides **1a** and **1b**, as generated by induced-fit docking into the human Y_4R model built based on the cryo-EM structure of the ternary complex hPP-hY_4R-G_{i1} (PDB-ID: 7X9C[51]). (C, D) Electrostatic contacts (salt bridges ❍) of the modified di-arginine motif of two picomolar cyclopeptide ligands of the Y_4R, as generated by induced-fit docking into a Y_4R homology model, reported recently.[5] The side chain of Y^{36} is involved in hydrophobic interactions with W6.48.

the intermolecular contacts within the binding pocket, further stabilize the ligand−receptor complex.

CONCLUSIONS

In this work, we have presented two α,γ-peptide analogues of the Y_4R-selective partial agonist UR-KK236, which contain the phenyl-cyclobutyl-γ-residue (1*R*,2*S*,3*R*)-γ-CBAA or its enantiomer at position 32. We show that the stereochemistry of the γ-residue at this position can influence both the free and the induced-fit conformations of the conserved di-arginine motif R^{33}-X-R^{35} of the NPY family: indeed, the (1*S*,2*R*,3*S*)-configuration renders the peptide bond L^{34}−R^{35} less susceptible toward ACE than the (1*R*,2*S*,3*R*)-configuration, but the latter results in a ligand with stronger Y_4R binding. However, the intrinsic agonistic activity is about half, which implies that the ligand does not properly induce the conformational changes of the receptor required for maximum activation. This is supported by the observation that the induced-fit conformation displays a significant number of intermolecular contacts that differ from those identified in the complex hPP-Y_4R-G_{i1} (Figures 1A and 9A,B). This concerns not only the salt-bridge and H-bond networks of R^{33} and R^{35} but also the role of the amino-acid residue at position 34: the latter is proline in the natural ligand hPP, which is involved in hydrophobic packing against the TM helices II and VII,[51] whereas it is L^{34} in **1a** and **1b**, which rather interacts with the TM helices IV and V (**1a**) or III and IV (**1b**) (Figure 7).

Recently, two backbone-to-side-chain cyclized analogues of UR-KK236 with picomolar Y_4R affinity have been reported:[5] the intrinsic agonistic activity of these cyclopeptides in different functional assays is lower than that of hPP but tends to be higher than that of the linear α-peptides UR-KK236 and UR-AK32,[4,5] and of the α,γ-peptides **1a** and **1b**. For example, in the Ca^{2+}-aequorin assay, intrinsic activities of 82−84%,[5] 75%,[4] and 54%[4] were measured, respectively, for the two cyclopeptides, UR-KK236 and UR-AK32. Interestingly, the receptor binding poses of the cyclopeptides, obtained from MD simulations, exhibit the characteristic salt bridges of the hPP di-arginine motif (R^{33} with E6.58$^{(288)}$, and R^{35} with D6.59$^{(289)}$, Figure 9C,D). However, the C-terminal amide group is not involved in the typical polar contacts with T2.61, Q3.32, and H7.39, which have been proven to be important for Y_4R activation upon hPP binding (Figure 1A).[51] Furthermore, L^{34} makes contacts mainly with the TM helices II and III, in contrast to hPP's P^{34}, which is packed against the TM helices II and VII. Therefore, reproducing the interactions of the hPP segment 32−36, especially of the conserved NPY/PP di-arginine motif and the C-terminal amide group, with the Y_4R is not a prerequisite to attain a strong binding, but it is important for high receptor activation.

Due to the therapeutic potential of small-to-medium-sized molecules with Y_4R agonism, e.g., for the treatment of obesity,[76,77] future investigations should focus on the structural properties that determine partial vs full Y_4R agonism, together with the respective mechanisms of receptor activation. In principle, compounds with full or partial agonistic activity are both pharmacologically and medicinally interesting,[78,79] but it should be considered that they act differently: for an exogenous full agonist, maximal receptor stimulation is expected, in analogy with the endogenous full agonist, while the behavior of an exogenous partial agonist is more complex, similar to that of an agonist−antagonist bifunctional molecule.[80] In fact, in a system with low basal receptor activity due to endogenous full agonist

https://doi.org/10.1021/acs.jmedchem.3c00363
J. Med. Chem. 2023, 66, 9642−9657

Downloaded from pubs.acs.org/jmcmar/article-pdf/66/14/9642/4587513/jm3c00363.pdf by FREIE UNIV BERLIN user on 14 November 2026

deficiency, an exogenous partial agonist will induce a submaximal receptor response; conversely, in a system where the receptor is already activated by the endogenous full agonist, an exogenous partial agonist will exert an antagonist-like effect resulting in reduced receptor response.[80] Therefore, a partial agonist has the advantage of excluding receptor overstimulation, which can occur upon administration of a full agonist developing side effects such as desensitization and dependence, but it requires a careful evaluation of its pharmacological impact on receptor stimulation.

EXPERIMENTAL SECTION

General Information. All chemicals were purchased and used as received, except for ethyl acetate and hexanes, which were distilled prior to use. High-resolution mass spectrometry (HR-MS) analyses were performed on an Agilent Technologies 6540 UHD Accurate-Mass Q-TOF LC/MS system. Chiral normal-phase (NP)-HPLC analysis was performed on a Varian 920-LC system with a diode array detector DAD (chiral stationary phase). RP-HPLC analysis was carried out on a Thermo Fisher Scientific Dionex UltiMate 3000 UHPLC system, a Shimadzu LC20A series instrument with a Shimadzu SPD-M20A UV−Vis detector, or an Agilent Technologies 1290 Infinity system with a 1260 Infinity diode array or a fluorescence detector.

γ-Amino Acids Synthesis. The N$^{\gamma}$-Fmoc protected (1*R*,2*S*,3*R*)-γ-CBAA and (1*S*,2*R*,3*S*)-γ-CBAA were prepared according to the literature procedure[55] (for ^{1}H and ^{13}C NMR spectra, see the Supporting Information).

Solid-Phase Peptide Synthesis and Purification. The linear peptides were synthesized manually by Fmoc-based SPPS on Rink-amide MBHA polystyrene/1% divinylbenzene resin (loading 0.58 mmol/g). The Fmoc-deprotection was carried out with 25% piperidine in *N*,*N*-dimethylformamide (DMF)/*N*-methyl-2-pyrrolidinone (NMP) (70:30, v/v) for 3 min and 12.5% piperidine in DMF/NMP (70:30, v/v) for 12 min. The double couplings (2 × 40 min) of the proteinogenic amino acids Fmoc-R(Pbf)-OH, Fmoc-Y(tBu)-OH, and Fmoc-L-OH were accomplished with the Fmoc-AA-OH/HOBt/HBTU/DIPEA mixture (5:5:4.8:10 equiv). The cyclic amino acids Fmoc-(1*S*,2*R*,3*S*)-γ-CBAA-OH and Fmoc-(1*R*,2*S*,3*R*)-γ-CBAA-OH were coupled by using a double coupling (2 × 1.5 h) with Fmoc-γ-CBAA-OH/HOBt/HBTU/DIPEA (4/4/3.8/8 equiv). *N*-terminal acetylation was performed with acetic anhydride/DIPEA (10:10 equiv) in DMF for 30 min. The side chains were deprotected, and the peptides were cleaved from the resin with TFA/H_2O/TIA/EDT/TIS (90:1:3:3:3, v/v/v/v/v, V_{tot} = 1 mL) for 3 h, precipitated by ice-cold diethyl ether, recovered by centrifugation at 4 °C for 5 min, washed three times with cold diethyl ether, and dried under nitrogen. The homogeneity and identification of the desired peptides were assessed by analytical RP-HPLC and MALDI-TOF-MS: analytical RP-HPLC was performed on a Syncronis C18 column (100 Å, 5 μm, 250 mm × 4.6 mm, Thermo Fisher Scientific) using the Thermo Fisher Scientific Dionex UltiMate 3000 UHPLC system (Germering, Germany). The UV detection was set at 220 nm. The products were dissolved in MeCN/H_2O (10:90, v/v) containing 0.1% TFA. The binary elution system consisted of (solvent A) 0.06% (v/v) TFA in water and (solvent B) 0.05% (v/v) TFA in MeCN. Analytical chromatograms were obtained with the following gradient: 1% solvent B for 8 min, then 50% solvent B over 35 min, at a flow rate of 1.5 mL /min. Mass spectra were recorded on an Autoflex Speed MALDI-TOF-MS (Bruker Daltonics, Bremen, Germany) by using α-cyano-4-hydroxycinnamic acid as a matrix.

The crude peptides were purified by preparative RP-HPLC on a Shimadzu LC20A series instrument with a Shimadzu SPD-M20A UV−VIS detector. The collected fractions were lyophilized using a Christ α 1−4 LD apparatus equipped with a vacuum pump (Vacuubrand RZ 6 rotary vane).

Characterization of the α,γ-Peptides. The purity of all peptides (≥95%) was determined by analytical RP-HPLC on a Shimadzu LC20A series instrument with a Shimadzu SPD-M20A UV−Vis detector (Figures S1 and S2). The chemical structures of peptides were confirmed by HR-MS on an Agilent 6540 UHD Accurate-Mass Q-TOF LC/MS system (Agilent Technologies) using a + ESI ionization source (Figures S1 and S2) and 2D-NMR spectroscopy (Tables S3−S11).

Ac-{R-[(1R,2S,3R)-γ-CBAA]-R-L-R-Y}-NH$_2$ ***(1a)***. The peptide was purified by preparative RP-HPLC on a Nucleodur 100−5 C18ec column (100 Å, 5 μm, 250 mm × 10 mm, Macherey-Nagel) using the following method: flow rate of 5 mL/min, UV detection at 220 nm, 40 °C, gradient: 0−23 min, 0.05% aqueous TFA/0.05% TFA in MeCN 90:10−75:25, t_r = 19.8 min. After lyophilization of the collected fractions, peptide **1a** was afforded as a white fluffy solid. The purity of the peptide was determined by analytical RP-HPLC analysis with a Nucleodur 100−5 C18ec column (100 Å, 5 μm, 250 mm × 4 mm, Macherey-Nagel) using the following method: flow rate of 0.8 mL/min, UV detection at 220 nm, 40 °C, gradient: 0−40 min, 0.05% aqueous TFA/0.05% TFA in MeCN 90:10−40:60, t_r = 16.8 min, 99%; HR-MS: (ESI-MS) *m*/*z* calcd for $[C_{47}H_{75}N_{16}O_8]^+$ $[M + H]^+$ 991.5948, found 991.5937, *m*/*z* calcd for $[C_{47}H_{76}N_{16}O_8]^{2+}$ $[M + 2H]^{2+}$ 496.3011, found 496.3020, *m*/*z* calcd for $[C_{47}H_{77}N_{16}O_8]^{3+}$ $[M + 3H]^{3+}$ 331.2031, found 331.2040.

Ac-{R-[(1S,2R,3S)-γ-CBAA]-R-L-R-Y}-NH$_2$ ***(1b)***. The peptide was purified by preparative RP-HPLC on a Nucleodur 100−5 C18ec column (100 Å, 5 μm, 250 mm × 10 mm, Macherey-Nagel) using the following method: flow rate of 5 mL/min, UV detection at 220 nm, 40 °C, gradient: 0−23 min, 0.05% aqueous TFA/0.05% TFA in MeCN 90:10−70:30, t_r = 16.0 min. After lyophilization of the collected fractions, peptide **1b** was afforded as a white fluffy solid. The purity of the peptide was determined by analytical RP-HPLC analysis with a Nucleodur 100−5 C18ec column (100 Å, 5 μm, 250 mm × 4 mm, Macherey-Nagel) using the following method: flow rate of 0.8 mL/min, UV detection at 220 nm, 40 °C, gradient: 0−40 min, 0.05% aqueous TFA/0.05% TFA in MeCN 90:10−40:60, t_r = 16.3 min, 98%; HR-MS: (ESI-MS) *m*/*z* calcd for $[C_{47}H_{76}N_{16}O_8]^{2+}$ $[M + 2H]^{2+}$ 496.3011, found 496.3009, *m*/*z* calcd for $[C_{47}H_{77}N_{16}O_8]^{3+}$ $[M + 3H]^{3+}$ 331.2031, found 331.2045.

Ac-{R-[(1R,2S,3R)-γ-CBAA]-R-[(1R,2S,3R)-γ-CBAA]-R-Y}-NH$_2$ ***(2a)***. The peptide was purified by preparative RP-HPLC on a Nucleodur 100−5 C18ec column (100 Å, 5 μm, 250 mm × 10 mm, Macherey-Nagel) using the following method: flow rate of 5 mL/min, UV detection at 220 nm, 40 °C, gradient: 0−25 min, 0.05% aqueous TFA/0.05% TFA in MeCN 90:10−65:35, t_r = 17.2 min. After lyophilization of the collected fractions, peptide **2a** was afforded as a white fluffy solid. The purity of the peptide was determined by analytical RP-HPLC analysis with a Nucleodur 100−5 C18ec column (100 Å, 5 μm, 250 mm × 4 mm, Macherey-Nagel) using the following method: flow rate of 0.8 mL/min, UV detection at 220 nm, 40 °C, gradient: 0−40 min, 0.05% aqueous TFA/0.05% TFA in MeCN 90:10−40:60, t_r = 18.6 min, >99%; HR-MS: (ESI-MS) *m*/*z* calcd for $[C_{53}H_{78}N_{16}O_8]^{2+}$ $[M + 2H]^{2+}$ 533.3089, found 533.3091, *m*/*z* calcd for $[C_{53}H_{79}N_{16}O_8]^{3+}$ $[M + 3H]^{3+}$ 355.8750, found 355.8756.

Ac-{R-[(1S,2R,3S)-γ-CBAA]-R-[(1S,2R,3S)-γ-CBAA]-R-Y}-NH$_2$ ***(2b)***. The peptide was purified by preparative RP-HPLC on a Nucleodur 100−5 C18ec column (100 Å, 5 μm, 250 mm × 10 mm, Macherey-Nagel) using the following method: flow rate of 5 mL/min, UV detection at 220 nm, 40 °C, gradient: 0−25 min, 0.05% aqueous TFA/0.05% TFA in MeCN 90:10−65:35, t_r = 17.9 min. After lyophilization of the collected fractions, peptide **2b** was afforded as a white fluffy solid. The purity of the peptide was determined by analytical RP-HPLC analysis with a Nucleodur 100−5 C18ec column (100 Å, 5 μm, 250 mm × 4 mm, Macherey-Nagel) using the following method: flow rate of 0.8 mL/min, UV detection at 220 nm, 40 °C, gradient: 0−40 min, 0.05% aqueous TFA/0.05% TFA in MeCN 90:10−40:60, t_r = 19.5 min, 95%; HR-MS: (ESI-MS) *m*/*z* calcd for $[C_{53}H_{77}N_{16}O_8]^+$ $[M + H]^+$ 1065.6105, found 1065.6106, *m*/*z* calcd for $[C_{53}H_{78}N_{16}O_8]^{2+}$ $[M + 2H]^{2+}$ 533.3089, found 533.3094, *m*/*z* calcd for $[C_{53}H_{79}N_{16}O_8]^{3+}$ $[M + 3H]^{3+}$ 355.8750, found 355.8757.

Cell Culture. Cells were cultured in 75 cm^2 flasks (Sarstedt, Nümbrecht, Germany) in a humidified atmosphere (95% air, 5% CO_2) at 37 °C. SK-N-MC neuroblastoma cells (obtained from the American Type Culture Collection, ATCC HTB-10) were grown in EMEM

Downloaded from pubs.acs.org/jmcmar/article-pdf/66/14/9642/4587513/jm3c00363.pdf by FREIE UNIV BERLIN user on 14 November 2026

https://doi.org/10.1021/acs.jmedchem.3c00363
J. Med. Chem. 2023, 66, 9642−9657

supplemented with 5% fetal calf serum (FCS). CHO-hY_2R cells (obtained from Perkin Elmer Inc., Rodgau, Germany) were maintained in Ham's F-12 supplemented with 5% FCS and G418 (400 μg/mL). CHO-hY_4R-G_{qi5}-mtAEQ cells[49] were cultured in HAM's F-12 supplemented with 10% FCS, hygromycin (400 μg/mL), zeocin (250 μg/mL), and G418 (400 μg/mL). HEC-1B-hY_5R cells[81] were maintained in EMEM supplemented with 5% FCS and G418 (400 μg/mL). HEK293T-NlucN-mG_{si}/Y_4R-NlucC cells[56] were cultivated in DMEM supplemented with 10% FCS, puromycin (1 μg/mL), and G418 (600 μg/mL).

Mini-G_{si} Protein Recruitment Assay (Agonist Mode). The assay was performed with HEK293T-NlucN-mini-G_{si}/Y_4R-NlucC cells as described elsewhere[56] with the following modification: the preparation of serial dilutions and the addition of the compounds of interest to the cells were not performed in the dark. Data were processed with GraphPad Prism 5 (GraphPad Software, San Diego, CA) as described elsewhere,[56] but the area under the curve was used instead of the peak or plateau value of the recorded signal.

Radioligand Binding Assays. The used radioligand binding assays were recently validated by the determination of binding affinities of the reference ligands pNPY (Y_1R, Y_2R, and Y_5R, Figure S4) and hPP (Y_4R, Table 1 and Figure 2A), being in good agreement with previously reported binding affinities for pNPY and hPP.[5,35] All radioligand competition binding studies were performed at intact cells at 23 ± 1 °C. **Y_1R binding**. Competition binding experiments at Y_1R-expressing SK-N-MC neuroblastoma cells were performed as described previously[33] using the radioligand [^{3}H]UR-MK299 (K_d = 0.044 nM, concentration: 0.15 nM). Due to low radioligand displacement, no curve fitting was performed for compounds **1b**, **2a**, and **2b** (Figure S4). Specific radioligand binding (nonspecific binding subtracted from total binding), obtained from competition binding experiments with **1a** (Figure S4), was normalized (100% = specifically bound radioligand in the absence of a competitor), plotted as % over log(concentration of a competitor), and analyzed by a four-parameter logistic fit (GraphPad Prism 5) to obtain pIC_{50} values, which were converted to pK_i values according to the Cheng−Prusoff equation[82] (logarithmic form). **Y_2R binding**. Competition binding experiments at CHO-hY_2R cells were performed as previously reported[4] using the radioligand [^{3}H]-propionyl-pNPY (K_d = 0.14 nM, concentration: 0.5 nM). Due to low radioligand displacement, no curve fitting was performed for the studied compounds **1a**, **1b**, **2a**, and **2b** (Figure S4). **Y_4R binding**. Competition binding experiments at CHO-hY_4R-G_{qi5}-mtAEQ cells were performed as described previously[5] using the radioligand [^{3}H]UR-KK200 (K_d = 0.67 nM, concentration: 1.0 nM).[35] Specific radioligand binding (nonspecific binding subtracted from total binding), obtained from competition binding experiments with **1a**, **1b**, **2a**, and **2b**, was normalized (100% = specifically bound radioligand in the absence of a competitor), plotted as % over log(concentration of a competitor) and analyzed by a four-parameter logistic fit (GraphPad Prism 5; in the case of **2b**, the bottom plateau of the curve was constrained to >0) to obtain pIC_{50} values, which were converted to pK_i values according to the Cheng−Prusoff equation[82] (logarithmic form). **Y_5R binding**. Competition binding experiments at HEC-1B-hY_5R cells were performed as described previously[35] using the radioligand [^{3}H]propionyl-pNPY (K_d = 11 nM, concentration: 5 nM).[57] Due to low radioligand displacement, no curve fitting was performed for the studied compounds **1a**, **1b**, **2a**, and **2b** (Figure S4).

Stability in Human Blood Plasma. The investigation of the stabilities of UR-KK336, **1a**, and **1b** in human heparinized plasma was performed in triplicate at 37 °C following a described procedure.[83] Briefly, 1-methyl-D-tryptophan was used as an internal standard. The incubation was stopped after various times (UR-KK236: 30 min, 2, 3, 4, 6, and 24 h; **1a**: 10 min, 30 min, 1, 2, 4, 6, and 24 h; **1b**: 30 min, 2, 4, 6, and 24 h). The samples were analyzed by analytical RP-HPLC using an HPLC system from Agilent Technologies (Santa Clara, CA) composed of a 1290 Infinity binary pump equipped with a degasser, a 1290 Infinity autosampler, a 1290 Infinity thermostated column compartment, a 1260 Infinity diode array detector, and a 1260 Infinity fluorescence detector. A Kinetex-XB C18 column, 2.6 μm, 100 mm × 3 mm (Phenomenex, Aschaffenburg, Germany), was used at a flow rate of 0.6 mL/min. UV detection was performed at 220 nm, and the column compartment temperature was 25 °C. Mixtures of MeCN (A) and 0.04% aqueous TFA (B) were used as mobile phases. The following linear gradients were used: 0−14 min: A/B 5:95−25:75, 14−15 min: 25:75−95:5, and 15−19 min: 95:5 (isocratic). The injection volume was 20 μL. The obtained recoveries and the recovery ratios (peptide/internal standard) are summarized in Table S2 (Supporting Information). The major degradation products were identified by LC-HR-MS analysis using the following equipment: an Agilent 6540 UHD Accurate-Mass Q-TOF LC/MS system coupled to an Agilent 1290 analytical HPLC system; LC method: column: YMC Triart C18, 1.9 μm, 75 mm × 2 mm (YMC Europe GmbH, Dinslaken, Germany), column temperature: 40 °C, solvent/linear gradient: 0−10 min: 0.1% aqueous HCOOH/0.1% HCOOH in MeCN 100:0−60:40, 10−10.1 min: 60:40−2:98, 10.1−11.1 min: 2:98, flow: 0.6 mL/min.

CD Spectroscopy. The peptides were dissolved in 50 mM phosphate buffer (pH 7.3) or 30% TFE in phosphate buffer at concentrations ranging from 90 μM to 130 μM (all determined by the UV absorbance of tyrosine using the molar extinction coefficient of 1480 M^{-1} cm^{-1} at 276 nm).[84] The CD spectra were recorded on a Chirascan Plus spectrometer (Applied Photophysics) at 23 °C using a 1 mm quartz cell from Hellma Analytics. For each CD spectrum, three scans were accumulated using a step resolution of 1 nm, a bandwidth of 1 nm, and a time-per-point of 1 s. The CD spectrum of the solvent was subtracted, and the difference spectrum was normalized to express the ellipticity in mean-residue molar ellipticity, divided by 10^3 and represented in the graphs as $[\Theta]_R \times 10^{-3}$ (deg cm^2 $dmol^{-1}$).

2D-NMR Spectroscopy. The NMR spectra were recorded on a 600 MHz AVANCE III HD spectrometer (Bruker Biospin) equipped with a QXI (^{1}H/^{13}C/^{15}N/^{31}P) probe at 298 K. The samples were prepared in either D_2O (100 atom%D, Armar Europe) or 7% D_2O/93% H_2O and measured in 5 mm NMR tubes (TA, Armar Europe). Standard 2D-NMR spectra were recorded: ^{1}H-^{1}H TOCSY spectra with a mixing time of 120 ms, 1024 × 512 points, spectral widths of 12.9 and 8.33 ppm, 4 scans and a recycle delay of 1 s; an identical experiment with a mixing time of 12 ms served as a ^{1}H-^{1}H COSY; a ^{1}H-^{1}H ROESY with a mixing time of 200 ms, 2048 × 700 points, spectral widths of 12.9 and 10.0 ppm, 96 scans and a recycle delay of 1 s; a ^{1}H-^{13}C HSQC optimized for aliphatic side chains with 1024 × 400 points, spectral widths of 13.9 and 77.0 ppm, 128 or 160 scans, a recycle delay of 1 s, and a ^{13}C offset of 45 ppm; a ^{1}H-^{13}C HSQC optimized for aromatic side chains with 1024 × 128 points, spectral widths of 13.9 and 44.2 ppm, 128 or 160 scans, a recycle delay of 1.2 s, and a ^{13}C offset of 128 ppm. ^{1}H-^{15}N HSQC spectra were measured using 1024 × 128 points, spectral widths of 13.9 and 36.5 ppm, 96 scans, a recycle delay of 1 s, and a ^{15}N offset of 116 ppm. The spectra were referenced to 2,2-dimethyl-silapentane sulfonic acid (DSS) using an external sample of 0.5 mM DSS and 2 mM sucrose in H_2O/D_2O. Data were processed with Topspin 3.6 (Bruker Biospin) and analyzed using Sparky 3.115 (T. D. Goddard and D. G. Kneller, SPARKY 3, University of California, San Francisco).

NOE-Restrained Structure Calculations. NOE cross-peaks extracted from 2D ROESY spectra were categorized as small, medium, and strong (Table S11) and converted into distance restraints. Structure calculations based on torsion angle dynamics were conducted using CYANA.[85] The CYANA library file was extended to include both enantiomers of γ-CBAA (CBR and CBS), the N-terminal acetyl group (ACE), and the C-terminal amide (NH2). Coordinates for ACE and NH2 were extracted from the PDB structures 5MAS[86] and 1HJE,[87] respectively. Coordinates for CBR and CBS were extracted by using the Molecular Operating Environment (Chemical Computing Group Inc., Montreal, QC, Canada, H3A 2R7 2016). For each peptide, 200 structures were calculated, and the 20 structures with the best target function were selected for the structural ensemble (Table S12). The structures were analyzed, fitted, and illustrated using MolMol.[88]

Molecular Dynamics Simulations. A model of the human Y_4R was built based on the cryo-EM structure with PDB-ID 7X9C.[51] Missing loops were modeled with the MODELLER[89] tool in UCSF Chimera.[75,90] The N-termini and C-termini were truncated at Q^{35} and Q^{341}, respectively. Amino acids were modeled in their dominant protonation state at pH 7. AutoDock Vina[91] was used to generate initial

Downloaded from pubs.acs.org/jmcmar/article-pdf/66/14/9642/4587513/jm3c00363.pdf by FREIE UNIV BERLIN user on 14 November 2026

https://doi.org/10.1021/acs.jmedchem.3c00363
J. Med. Chem. 2023, 66, 9642−9657

poses of **1a** and **1b** in the human Y_4R model. A search space of 24 Å × 30 Å × 24 Å was used to ensure complete coverage of the binding pocket. The best-ranked pose was then selected for MD simulations. AmberTools18[92] was used to prepare the system for MD simulations. Missing hydrogen atoms were added, disulfide bonds were set, and N-termini and C-termini charges were generated with tleap. The topology for the receptor was generated using the AMBER99SB-ILDN force field.[93,94] A short energy minimization that comprised 500 steps of steepest descent and 4500 steps of the conjugate gradient optimization was conducted with a sander. The phenyl-cyclobutyl-γ-residue γ-CBAA in peptides **1a** and **1b** was prepared with AmberTools18.[92] Atom types and partial charges were assigned with antechamber. Prepgen was used to prepare the library of the γ-residue, and force-field parameters were assigned from ff99SB with parmchk2. The topologies for the peptides were generated using the AMBER99SB-ILDN force field. The receptor−peptide complex was inserted into a pre-equilibrated dioleoylphosphatidylcholine bilayer,[95] according to the orientation in the OPM database[96] using the GROMACS tool gmx membed.[97] The appropriate number of sodium and chloride ions was added to the systems to simulate a physiological salt concentration of 100 mM. Particle mesh Ewald (PME)[98] was used to treat electrostatic interactions, using a cut-off distance of 10 Å. The resulting systems were geometry-optimized and then equilibrated for 300 ns followed by a production run of 2 μs. All simulations used the SPC/E water model[99] and were performed using GROMACS 2021.5.[100] Analysis of the trajectories was performed with the CPPTRAJ module of AmberTools18.[92] Structural stability was analyzed by computing the RMSD, RMSF, and B-factors (Figures S12 and S13). The non-bonded interaction energy terms (electrostatic and Van der Waals) between the peptides and the receptor were calculated within the LIE methodology implemented in CPPTRAJ with the default 12 Å cut-off (Figures S15−S18). The trajectory snapshots were clustered using a hierarchical agglomerative approach with a minimum distance between clusters of 5.0 Å. For **1a** and **1b**, the most populated cluster was found predominantly in runs 3 and 2, respectively. Contacts were defined between any atom pair (including hydrogen atoms) with a maximum distance of 5 Å for the trajectory of the most populated cluster. UCSF Chimera[75,90] was used for data analysis and visualization, and plots were created with Matplotlib.[101]

■ ASSOCIATED CONTENT

Supporting Information

The Supporting Information is available free of charge at https://pubs.acs.org/doi/10.1021/acs.jmedchem.3c00363.

Experimental data; HPLC traces; mass spectra; NMR spectra; and additional tables and figures (PDF)

The PDB coordinates of the induced-fit docking poses of **1a** and **1b** along with the human Y_4R model are provided in the following PDB files: npy4_1a_Gi.pdb (docking of ligand **1a** into Y_4R) (PDB)

npy4_1b_Gi.pdb (docking of ligand **1b** into Y_4R) (PDB)

Molecular formula strings (CSV)

■ AUTHOR INFORMATION

Corresponding Authors

Max Keller − *Institute of Pharmacy, Faculty of Chemistry and Pharmacy, University of Regensburg, 93053 Regensburg, Germany;* orcid.org/0000-0002-8095-8627; Email: max.keller@ur.de

Chiara Cabrele − *Department of Biosciences and Medical Biology, University of Salzburg, 5020 Salzburg, Austria;* orcid.org/0000-0002-7550-6896; Email: chiara.cabrele@gmail.com

Timothy Clark − *Department of Chemistry and Pharmacy, Computer-Chemistry-Center, Friedrich-Alexander-University Erlangen-Nürnberg, 91052 Erlangen, Germany;* orcid.org/0000-0001-7931-4659; Email: tim.clark@fau.de

Oliver Reiser − *Institute of Organic Chemistry, Faculty of Chemistry and Pharmacy, University of Regensburg, 93053 Regensburg, Germany;* orcid.org/0000-0003-1430-573X; Email: oliver.reiser@ur.de

Authors

Eva Plut − *Institute of Organic Chemistry, Faculty of Chemistry and Pharmacy, University of Regensburg, 93053 Regensburg, Germany;* orcid.org/0000-0002-2630-7284

Jacqueline C. Calderón − *Department of Chemistry and Pharmacy, Computer-Chemistry-Center, Friedrich-Alexander-University Erlangen-Nürnberg, 91052 Erlangen, Germany*

Vesna Stanojlović − *Department of Biosciences and Medical Biology, University of Salzburg, 5020 Salzburg, Austria*

Albert O. Gattor − *Institute of Pharmacy, Faculty of Chemistry and Pharmacy, University of Regensburg, 93053 Regensburg, Germany;* orcid.org/0000-0001-5166-2168

Carina Höring − *Institute of Pharmacy, Faculty of Chemistry and Pharmacy, University of Regensburg, 93053 Regensburg, Germany*

Laura J. Humphrys − *Institute of Pharmacy, Faculty of Chemistry and Pharmacy, University of Regensburg, 93053 Regensburg, Germany;* orcid.org/0000-0003-4019-5538

Adam Konieczny − *Institute of Pharmacy, Faculty of Chemistry and Pharmacy, University of Regensburg, 93053 Regensburg, Germany*

Sabine Kerres − *Institute of Organic Chemistry, Faculty of Chemistry and Pharmacy, University of Regensburg, 93053 Regensburg, Germany*

Mario Schubert − *Department of Biosciences and Medical Biology, University of Salzburg, 5020 Salzburg, Austria;* orcid.org/0000-0003-0278-4091

Complete contact information is available at: https://pubs.acs.org/10.1021/acs.jmedchem.3c00363

Notes

The authors declare no competing financial interest.

■ ACKNOWLEDGMENTS

This work was supported by the DFG (GRK 1910: Medicinal Chemistry of selective GPCR ligands (E.P., J.C., A.O.G., C.H., L.J.H., and A.K.), GRK 1626 Photocatalysis (S.K.), RE948-9 (S.K.), and Friedrich-Ebert-Stiftung (S.K.). The authors gratefully acknowledge the scientific support and HPC resources provided by the Erlangen National High Performance Computing Center (NHR@FAU) of the Friedrich-Alexander-University Erlangen-Nürnberg (FAU) under an early-access NHR project. NHR funding is provided by Federal and Bavarian State authorities. NHR@FAU hardware is partially funded by the German Research Foundation (DFG)—440719683.

■ ABBREVIATIONS USED

BSA, bovine serum albumin; cryo-EM, cryogenic electron microscopy; DMEM, Dulbecco's modified eagle medium; ECL, extracellular loop; EMEM, Eagle's minimal essential medium; FCS, fetal calf serum; G418, geneticin; Nluc, nanoluciferase; NlucN, N-terminal fragment of the Nluc, 159 amino acids; NlucC, C-terminal fragment of the Nluc, 11 amino acids; PBS, phosphate buffer saline; RP-HPLC, reversed-phase high-performance liquid chromatography; TFA, trifluoroacetic acid

Downloaded from pubs.acs.org/jmcmar/article-pdf/66/14/9642/4587513/jm3c00363.pdf by FREIE UNIV BERLIN user on 14 November 2026

REFERENCES

(1) Cabrele, C.; Beck-Sickinger, A. G. Molecular Characterization of the Ligand-Receptor Interaction of the Neuropeptide Y Family. *J. Pept. Sci.* **2000**, *6*, 97−122.

(2) Holzer, P.; Reichmann, F.; Farzi, A. Neuropeptide Y, Peptide YY and Pancreatic Polypeptide in the Gut−Brain Axis. *Neuropeptides* **2012**, *46*, 261−274.

(3) Keire, D. A.; Bowers, C. W.; Solomon, T. E.; Reeve, J. R. Structure and Receptor Binding of PYY Analogs. *Peptides* **2002**, *23*, 305−321.

(4) Konieczny, A.; Braun, D.; Wifling, D.; Bernhardt, G.; Keller, M. Oligopeptides as Neuropeptide Y Y_4 Receptor Ligands: Identification of a High-Affinity Tetrapeptide Agonist and a Hexapeptide Antagonist. *J. Med. Chem.* **2020**, *63*, 8198−8215.

(5) Konieczny, A.; Conrad, M.; Ertl, F. J.; Gleixner, J.; Gattor, A. O.; Grätz, L.; Schmidt, M. F.; Neu, E.; Horn, A. H. C.; Wifling, D.; et al. N-Terminus to Arginine Side-Chain Cyclization of Linear Peptidic Neuropeptide Y Y_4 Receptor Ligands Results in Picomolar Binding Constants. *J. Med. Chem.* **2021**, *64*, 16746−16769.

(6) Walther, C.; Mörl, K.; Beck-Sickinger, A. G. Neuropeptide Y Receptors: Ligand Binding and Trafficking Suggest Novel Approaches in Drug Development. *J. Pept. Sci.* **2011**, *17*, 233−246.

(7) Hoppenz, P.; Els-Heindl, S.; Beck-Sickinger, A. G. Peptide-Drug Conjugates and Their Targets in Advanced Cancer Therapies. *Front. Chem.* **2020**, *8*, 571.

(8) Körner, M.; Reubi, J. C. NPY Receptors in Human Cancer: A Review of Current Knowledge. *Peptides* **2007**, *28*, 419−425.

(9) Li, J.; Tian, Y.; Wu, A. Neuropeptide Y Receptors: A Promising Target for Cancer Imaging and Therapy. *Regen. Biomater.* **2015**, *2*, 215−219.

(10) Brothers, S. P.; Wahlestedt, C. Therapeutic Potential of Neuropeptide Y (NPY) Receptor Ligands. *EMBO Mol. Med.* **2010**, *2*, 429−439.

(11) Loh, K.; Herzog, H.; Shi, Y.-C. Regulation of Energy Homeostasis by the NPY System. *Trends Endocrinol. Metab.* **2015**, *26*, 125−135.

(12) Duarte-Neves, J.; Pereira de Almeida, L.; Cavadas, C. Neuropeptide Y (NPY) as a Therapeutic Target for Neurodegenerative Diseases. *Neurobiol. Dis.* **2016**, *95*, 210−224.

(13) Tan, C. M. J.; Green, P.; Tapoulal, N.; Lewandowski, A. J.; Leeson, P.; Herring, N. The Role of Neuropeptide Y in Cardiovascular Health and Disease. *Front. Physiol.* **2018**, *9*, 1281.

(14) Enman, N. M.; Sabban, E. L.; McGonigle, P.; van Bockstaele, E. J. Targeting the Neuropeptide Y System in Stress-Related Psychiatric Disorders. *Neurobiol. Stress* **2015**, *1*, 33−43.

(15) Heilig, M. The NPY System in Stress, Anxiety and Depression. *Neuropeptides* **2004**, *38*, 213−224.

(16) Hirsch, D.; Zukowska, Z. NPY and Stress 30 Years Later: The Peripheral View. *Cell. Mol. Neurobiol.* **2012**, *32*, 645−659.

(17) Reichmann, F.; Holzer, P. Neuropeptide Y: A Stressful Review. *Neuropeptides* **2016**, *55*, 99−109.

(18) Sah, R.; Geracioti, T. D. Neuropeptide Y and Posttraumatic Stress Disorder. *Mol. Psychiatry* **2013**, *18*, 646−655.

(19) Morales-Medina, J. C.; Dumont, Y.; Benoit, C.-E.; Bastianetto, S.; Flores, G.; Fournier, A.; Quirion, R. Role of Neuropeptide Y Y_1 and Y_2 Receptors on Behavioral Despair in a Rat Model of Depression with Co-Morbid Anxiety. *Neuropharmacology* **2012**, *62*, 200−208.

(20) Morales-Medina, J. C.; Dumont, Y.; Quirion, R. A Possible Role of Neuropeptide Y in Depression and Stress. *Brain Res.* **2010**, *1314*, 194−205.

(21) Wu, G.; Feder, A.; Wegener, G.; Bailey, C.; Saxena, S.; Charney, D.; Mathé, A. A. Central Functions of Neuropeptide Y in Mood and Anxiety Disorders. *Expert Opin. Ther. Targets* **2011**, *15*, 1317−1331.

(22) Antal-Zimanyi, I.; Bruce, M. A.; LeBoulluec, K. L.; Iben, L. G.; Mattson, G. K.; McGovern, R. T.; Hogan, J. B.; Leahy, C. L.; Flowers, S. C.; Stanley, J. A.; et al. Pharmacological Characterization and Appetite Suppressive Properties of BMS-193885, a Novel and Selective Neuropeptide Y_1 Receptor Antagonist. *Eur. J. Pharmacol.* **2008**, *590*, 224−232.

(23) Balasubramaniam, A.; Dhawan, V. C.; Mullins, D. E.; Chance, W. T.; Sheriff, S.; Guzzi, M.; Prabhakaran, M.; Parker, E. M. Highly Selective and Potent Neuropeptide Y (NPY) Y_1 Receptor Antagonists Based on Pro^{30}, Tyr^{32}, Leu^{34}NPY(28-36)-NH_2 (BW1911U90). *J. Med. Chem.* **2001**, *44*, 1479−1482.

(24) Balasubramaniam, A.; Mullins, D. E.; Lin, S.; Zhai, W.; Tao, Z.; Dhawan, V. C.; Guzzi, M.; Knittel, J. J.; Slack, K.; Herzog, H.; Parker, E. M. Neuropeptide Y (NPY) Y_4 Receptor Selective Agonists Based on NPY(32-36): Development of an Anorectic Y_4 Receptor Selective Agonist with Picomolar Affinity. *J. Med. Chem.* **2006**, *49*, 2661−2665.

(25) Balasubramaniam, A.; Zhai, W.; Sheriff, S.; Tao, Z.; Chance, W. T.; Fischer, J. E.; Eden, P.; Taylor, J. Bis(31/31′)-(Cys[31], Trp[32], Nva[34] NPY-(31-36)): A Specific NPY Y-1 Receptor Antagonist. *J. Med. Chem.* **1996**, *39*, 811−813.

(26) Cabrele, C.; Langer, M.; Bader, R.; Wieland, H. A.; Doods, H. N.; Zerbe, O.; Beck-Sickinger, A. G. The First Selective Agonist for the Neuropeptide YY_5 Receptor Increases Food Intake in Rats. *J. Biol. Chem.* **2000**, *275*, 36043−36048.

(27) Cippitelli, A.; Rezvani, A. H.; Robinson, J. E.; Eisenberg, L.; Levin, E. D.; Bonaventure, P.; Motley, S. T.; Lovenberg, T. W.; Heilig, M.; Thorsell, A. The Novel, Selective, Brain-Penetrant Neuropeptide Y Y_2 Receptor Antagonist, JNJ-31020028, Tested in Animal Models of Alcohol Consumption, Relapse, and Anxiety. *Alcohol* **2011**, *45*, 567−576.

(28) Daniels, A. J.; Matthews, J. E.; Slepetis, R. J.; Jansen, M.; Viveros, O. H.; Tadepalli, A.; Harrington, W.; Heyer, D.; Landavazo, A.; Leban, J. J.; et al. High-Affinity Neuropeptide Y Receptor Antagonists. *Proc. Natl. Acad. Sci. U.S.A.* **1995**, *92*, 9067−9071.

(29) Doods, H.; Gaida, W.; Wieland, H. A.; Dollinger, H.; Schnorrenberg, G.; Esser, F.; Engel, W.; Eberlein, W.; Rudolf, K. BIIE0246: A Selective and High Affinity Neuropeptide Y Y_2 Receptor Antagonist. *Eur. J. Pharmacol.* **1999**, *384*, R3−R5.

(30) Erondu, N.; Gantz, I.; Musser, B.; Suryawanshi, S.; Mallick, M.; Addy, C.; Cote, J.; Bray, G.; Fujioka, K.; Bays, H.; et al. Neuropeptide Y_5 Receptor Antagonism Does Not Induce Clinically Meaningful Weight Loss in Overweight and Obese Adults. *Cell Metab.* **2006**, *4*, 275−282.

(31) Hofmann, S.; Lindner, J.; Beck-Sickinger, A. G.; Hey-Hawkins, E.; Bellmann-Sickert, K. Carbaboranylation of Truncated C-Terminal Neuropeptide Y Analogue Leads to Full hY_1 Receptor Agonism. *ChemBioChem* **2018**, *19*, 2300−2306.

(32) Keller, M.; Kaske, M.; Holzammer, T.; Bernhardt, G.; Buschauer, A. Dimeric Argininamide-Type Neuropeptide Y Receptor Antagonists: Chiral Discrimination Between Y_1 and Y_4 receptors. *Biorg. Med. Chem.* **2013**, *21*, 6303−6322.

(33) Keller, M.; Weiss, S.; Hutzler, C.; Kuhn, K. K.; Mollereau, C.; Dukorn, S.; Schindler, L.; Bernhardt, G.; König, B.; Buschauer, A. N(ω)-Carbamoylation of the Argininamide Moiety: An Avenue to Insurmountable NPY Y_1 Receptor Antagonists and a Radiolabeled Selective High-Affinity Molecular Tool ([^{3}H]UR-MK299) with Extended Residence Time. *J. Med. Chem.* **2015**, *58*, 8834−8849.

(34) Koglin, N.; Zorn, C.; Beumer, R.; Cabrele, C.; Bubert, C.; Sewald, N.; Reiser, O.; Beck-Sickinger, A. G. Analogues of Neuropeptide Y Containing Beta-Aminocyclopropane Carboxylic Acids Are the Shortest Linear Peptides That Are Selective for the Y_1 Receptor. *Angew. Chem., Int. Ed.* **2003**, *42*, 202−205.

(35) Kuhn, K. K.; Ertl, T.; Dukorn, S.; Keller, M.; Bernhardt, G.; Reiser, O.; Buschauer, A. High Affinity Agonists of the Neuropeptide Y (NPY) Y_4 Receptor Derived from the C-Terminal Pentapeptide of Human Pancreatic Polypeptide (hPP): Synthesis, Stereochemical Discrimination, and Radiolabeling. *J. Med. Chem.* **2016**, *59*, 6045−6058.

(36) Kuhn, K. K.; Littmann, T.; Dukorn, S.; Tanaka, M.; Keller, M.; Ozawa, T.; Bernhardt, G.; Buschauer, A. In Search of NPY Y_4R Antagonists: Incorporation of Carbamoylated Arginine, Aza-Amino Acids, or D-Amino Acids into Oligopeptides Derived from the C-Termini of the Endogenous Agonists. *ACS Omega* **2017**, *2*, 3616−3631.

(37) Liu, M.; Mountford, S. J.; Richardson, R. R.; Groenen, M.; Holliday, N. D.; Thompson, P. E. Optically Pure, Structural, and

Downloaded from pubs.acs.org/jmcmar/article-pdf/66/14/9642/4587513/jm3c00363.pdf by FREIE UNIV BERLIN user on 14 November 2026

https://doi.org/10.1021/acs.jmedchem.3c00363
J. Med. Chem. 2023, 66, 9642−9657

Fluorescent Analogues of a Dimeric Y_4 Receptor Agonist Derived by an Olefin Metathesis Approach. *J. Med. Chem.* **2016**, *59*, 6059−6069.
(38) MacNeil, D. J. NPY Y_1 and Y_5 Receptor Selective Antagonists as Anti-Obesity Drugs. *Curr. Top. Med. Chem.* **2007**, *7*, 1721−1733.
(39) Parker, E. M.; Babij, C. K.; Balasubramaniam, A.; Burrier, R. E.; Guzzi, M.; Hamud, F.; Mukhopadhyay, G.; Rudinski, M. S.; Tao, Z.; Tice, M.; et al. GR231118 (1229U91) and Other Analogues of the C-Terminus of Neuropeptide Y Are Potent Neuropeptide Y Y_1 Receptor Antagonists and Neuropeptide Y Y_4 Receptor Agonists. *Eur. J. Pharmacol.* **1998**, *349*, 97−105.
(40) Richardson, R. R.; Groenen, M.; Liu, M.; Mountford, S. J.; Briddon, S. J.; Holliday, N. D.; Thompson, P. E. Heterodimeric Analogues of the Potent Y_1R Antagonist 1229U91, Lacking One of the Pharmacophoric C-Terminal Structures, Retain Potent Y_1R Affinity and Show Improved Selectivity over Y_4R. *J. Med. Chem.* **2020**, *63*, 5274−5286.
(41) Rudolf, K.; Eberlein, W.; Engel, W.; Wieland, H. A.; Willim, K. D.; Entzeroth, M.; Wienen, W.; Beck-Sickinger, A. G.; Doods, H. N. The First Highly Potent and Selective Non-Peptide Neuropeptide Y Y_1 Receptor Antagonist: BIBP3226. *Eur. J. Pharmacol.* **1994**, *271*, R11−R13.
(42) Schubert, M.; Stichel, J.; Du, Y.; Tough, I. R.; Sliwoski, G.; Meiler, J.; Cox, H. M.; Weaver, C. D.; Beck-Sickinger, A. G. Identification and Characterization of the First Selective Y_4 Receptor Positive Allosteric Modulator. *J. Med. Chem.* **2017**, *60*, 7605−7612.
(43) Schüß, C.; Vu, O.; Schubert, M.; Du, Y.; Mishra, N. M.; Tough, I. R.; Stichel, J.; Weaver, C. D.; Emmitte, K. A.; Cox, H. M.; et al. Highly Selective Y_4 Receptor Antagonist Binds in an Allosteric Binding Pocket. *J. Med. Chem.* **2021**, *64*, 2801−2814.
(44) Shoblock, J. R.; Welty, N.; Nepomuceno, D.; Lord, B.; Aluisio, L.; Fraser, I.; Motley, S. T.; Sutton, S. W.; Morton, K.; Galici, R.; et al. In Vitro and in Vivo Characterization of JNJ-31020028 (N-(4-{4-2-(Diethylamino)-2-oxo-1-phenylethylpiperazin-1-yl}-3-fluorophenyl)-2-pyridin-3-ylbenzamide), a Selective Brain Penetrant Small Molecule Antagonist of the Neuropeptide Y Y_2 Receptor. *Psychopharmacology* **2010**, *208*, 265−277.
(45) Tang, T.; Hartig, C.; Chen, Q.; Zhao, W.; Kaiser, A.; Zhang, X.; Zhang, H.; Qu, H.; Yi, C.; Ma, L.; et al. Structural Basis for Ligand Recognition of The Neuropeptide Y Y_2 Receptor. *Nat. Commun.* **2021**, *12*, No. 737.
(46) Walker, M. W.; Wolinsky, T. D.; Jubian, V.; Chandrasena, G.; Zhong, H.; Huang, X.; Miller, S.; Hegde, L. G.; Marsteller, D. A.; Marzabadi, M. R.; et al. The Novel Neuropeptide Y Y_5 Receptor Antagonist Lu AA33810 [N-[[*trans*-4-[(4,5-Dihydro[1]-benzothiepino[5,4-d]thiazol-2-yl)amino]cyclohexyl]methyl]-methanesulfonamide] Exerts Anxiolytic- and Antidepressant-Like Effects in Rat Models of Stress Sensitivity. *J. Pharmacol. Exp. Ther.* **2009**, *328*, 900−911.
(47) Wieland, H. A.; Engel, W.; Eberlein, W.; Rudolf, K.; Doods, H. N. Subtype Selectivity of the Novel Nonpeptide Neuropeptide Y Y_1 Receptor Antagonist BIBO 3304 and Its Effect on Feeding in Rodents. *Br. J. Pharmacol.* **1998**, *125*, 549−555.
(48) Yang, Z.; Han, S.; Keller, M.; Kaiser, A.; Bender, B. J.; Bosse, M.; Burkert, K.; Kögler, L. M.; Wifling, D.; Bernhardt, G.; et al. Structural Basis of Ligand Binding Modes at the Neuropeptide Y Y_1 Receptor. *Nature* **2018**, *556*, 520−524.
(49) Ziemek, R.; Schneider, E.; Kraus, A.; Cabrele, C.; Beck-Sickinger, A. G.; Bernhardt, G.; Buschauer, A. Determination of Affinity and Activity of Ligands at the Human Neuropeptide Y Y_4 Receptor by Flow Cytometry and Aequorin Luminescence. *J. Recept. Signal Transduction Res.* **2007**, *27*, 217−233.
(50) Zwanziger, D.; Böhme, I.; Lindner, D.; Beck-Sickinger, A. G. First Selective Agonist of the Neuropeptide Y_1-Receptor with Reduced Size. *J. Pept. Sci.* **2009**, *15*, 856−866.
(51) Tang, T.; Tan, Q.; Han, S.; Diemar, A.; Löbner, K.; Wang, H.; Schüß, C.; Behr, V.; Mörl, K.; Wang, M.; et al. Receptor-Specific Recognition of NPY Peptides Revealed by Structures of NPY Receptors. *Sci. Adv.* **2022**, *8*, No. eabm1232. PDB doi: https://doi.org/10.2210/pdb7X9C/pdb
(52) Kimmel, J. R.; Hayden, L. J.; Pollock, H. G. Isolation and Characterization of a New Pancreatic Polypeptide Hormone. *J. Biol. Chem.* **1975**, *250*, 9369−9376.
(53) Tatemoto, K. Neuropeptide Y: Complete Amino Acid Sequence of the Brain Peptide. *Proc. Natl. Acad. Sci. U.S.A.* **1982**, *79*, 5485−5489.
(54) Berlicki, Ł.; Kaske, M.; Gutiérrez-Abad, R.; Bernhardt, G.; Illa, O.; Ortuño, R. M.; Cabrele, C.; Buschauer, A.; Reiser, O. Replacement of Thr^{32} and Gln^{34} in the C-Terminal Neuropeptide Y Fragment 25-36 by *cis*-Cyclobutane and *cis*-Cyclopentane *β*-Amino Acids Shifts Selectivity Toward the Y_4 Receptor. *J. Med. Chem.* **2013**, *56*, 8422−8431.
(55) Kerres, S.; Plut, E.; Malcherek, S.; Rehbein, J.; Reiser, O. Visible Light-Mediated Synthesis of Enantiopure *γ*-Cyclobutane Amino and 3-(Aminomethyl)-5-phenylpentanoic Acids. *Adv. Synth. Catal.* **2019**, *361*, 1400−1407.
(56) Wirth, U.; Erl, J.; Azzam, S.; Hoering, C.; Skiba, M.; Singh, R.; Hochmuth, K.; Keller, M.; Wegener, J.; König, B. Monitoring the Reversibility of GPCR Signaling by Combining Photochromic Ligands with Label-Free Impedance Analysis. *Angew. Chem., Int. Ed.* **2023**, No. e202215547.
(57) Dukorn, S.; Littmann, T.; Keller, M.; Kuhn, K.; Cabrele, C.; Baumeister, P.; Bernhardt, G.; Buschauer, A. Fluorescence- and Radiolabeling of [Lys^4,$Nle^{17,30}$]hPP Yields Molecular Tools for the NPY Y_4 Receptor. *Bioconjugate Chem.* **2017**, *28*, 1291−1304.
(58) Hubbard, S. J.; Beynon, R. J.; Thornton, J. M. Assessment of Conformational Parameters as Predictors of Limited Proteolytic Sites in Native Protein Structures. *Protein Eng. Des. Sel.* **1998**, *11*, 349−359.
(59) Haas, E.; Montelione, G. T.; McWherter, C. A.; Scheraga, H. A. Local Structures in a Tryptic Fragment of Performic Acid Oxidized Ribonuclease A Corresponding to a Proposed Polypeptide Chain Folding Initiation Site Detected by Tyrosine Fluorescence Lifetime and Proton Magnetic Resonance Measurements. *Biochemistry* **1987**, *26*, 1672−1683.
(60) Lester, C. C.; Xu, X.; Laity, J. H.; Shimotakahara, S.; Scheraga, H. A. Regeneration Studies of an Analog of Ribonuclease A Missing Disulfide Bonds 65−72 and 40−95. *Biochemistry* **1997**, *36*, 13068−13076.
(61) Swadesh, J. K.; Montelione, G. T.; Thannhauser, T. W.; Scheraga, H. A. Local Structure Involving Histidine-12 in Reduced S-Sulfonated Ribonuclease A Detected by Proton NMR Spectroscopy Under Folding Conditions. *Proc. Natl. Acad. Sci. U.S.A.* **1984**, *81*, 4606−4610.
(62) Buck, M. Trifluoroethanol and Colleagues: Cosolvents Come of Age. Recent Studies with Peptides and Proteins. *Q. Rev. Biophys.* **1998**, *31*, 297−355.
(63) Starzyk, A.; Barber-Armstrong, W.; Sridharan, M.; Decatur, S. M. Spectroscopic Evidence for Backbone Desolvation of Helical Peptides by 2,2,2-Trifluoroethanol: An Isotope-Edited FTIR Study. *Biochemistry* **2005**, *44*, 369−376.
(64) Uversky, V. N.; Narizhneva, N. V.; Kirschstein, S. O.; Winter, S.; Löber, G. Conformational Transitions Provoked by Organic Solvents in *β*-Lactoglobulin: Can a Molten Globule Like Intermediate Be Induced by the Decrease in Dielectric Constant? *Fold Des.* **1997**, *2*, 163−172.
(65) Vincenzi, M.; Mercurio, A. F.; Leone, M. About TFE: Old and New Findings. *Curr. Protein Pept. Sci.* **2019**, *20*, 425−451.
(66) Yu, Y.; Wang, J.; Shao, Q.; Shi, J.; Zhu, W. The Effects of Organic Solvents on the Folding Pathway and Associated Thermodynamics of Proteins: A Microscopic View. *Sci. Rep.* **2016**, *6*, No. 19500.
(67) Kiewitz, S. D.; Cabrele, C. Synthesis and Conformational Properties of Protein Fragments Based on the Id Family of DNA-Binding and Cell-Differentiation Inhibitors. *Biopolymers* **2005**, *80*, 762−774.
(68) Stanojlovic, V.; Müller, A.; Moazzam, A.; Hinterholzer, A.; Ożga, K.; Berlicki, Ł.; Schubert, M.; Cabrele, C. A Conformationally Stable Acyclic *β*-Hairpin Scaffold Tolerating the Incorporation of Poorly *β*-Sheet-Prone Amino Acids. *ChemBioChem* **2022**, *23*, No. e202100604.
(69) Platzer, G.; Okon, M.; McIntosh, L. P. pH-Dependent Random Coil ^1H, ^{13}C, and ^{15}N Chemical Shifts of the Ionizable Amino Acids: A Guide for Protein pK_a Measurements. *J. Biomol. NMR* **2014**, *60*, 109−129.

Downloaded from pubs.acs.org/jmcmar/article-pdf/66/14/9642/4587513/jm3c00363.pdf by FREIE UNIV BERLIN user on 14 November 2026

(70) Wishart, D. S.; Bigam, C. G.; Holm, A.; Hodges, R. S.; Sykes, B. D. ^{1}H, ^{13}C and ^{15}N Random Coil NMR Chemical Shifts of the Common Amino Acids. I. Investigations of Nearest-neighbor Effects. *J. Biomol. NMR* **1995**, *5*, 67−81.
(71) Karle, I. L.; Flippen-Anderson, J.; Sukumar, M.; Balaram, P. Conformation of a 16-Residue Zervamicin IIA Analog Peptide Containing Three Different Structural Features: 3_{10}-Helix, α-Helix, and β-Bend Ribbon. *Proc. Natl. Acad. Sci. U.S.A.* **1987**, *84*, 5087−5091.
(72) Dror, R. O.; Pan, A. C.; Arlow, D. H.; Borhani, D. W.; Maragakis, P.; Shan, Y.; Xu, H.; Shaw, D. E. Pathway and Mechanism of Drug Binding to G-Protein-Coupled Receptors. *Proc. Natl. Acad. Sci. U.S.A.* **2011**, *108*, 13118−13123.
(73) Mattedi, G.; Deflorian, F.; Mason, J. S.; Graaf, C.; Gervasio, F. L. Understanding Ligand Binding Selectivity in a Prototypical GPCR Family. *J. Chem. Inf. Model.* **2019**, *59*, 2830−2836.
(74) Goddard, T. D.; Huang, C. C.; Meng, E. C.; Pettersen, E. F.; Couch, G. S.; Morris, J. H.; Ferrin, T. E. UCSF ChimeraX: Meeting Modern Challenges in Visualization and Analysis. *Protein Sci.* **2018**, *27*, 14−25.
(75) Pettersen, E. F.; Goddard, T. D.; Huang, C. C.; Couch, G. S.; Greenblatt, D. M.; Meng, E. C.; Ferrin, T. E. UCSF Chimera—A Visualization System for Exploratory Research and Analysis. *J. Comput. Chem.* **2004**, *25*, 1605−1612.
(76) Li, J. B.; Asakawa, A.; Terashi, M.; Cheng, K.; Chaolu, H.; Zoshiki, T.; Ushikai, M.; Sheriff, S.; Balasubramaniam, A.; Inui, A. Regulatory Effects of Y_4 Receptor Agonist (BVD-74D) on Food Intake. *Peptides* **2010**, *31*, 1706−1710.
(77) Thieme, V.; Jolly, N.; Madsen, A. N.; Bellmann-Sickert, K.; Schwartz, T. W.; Holst, B.; Cox, H. M.; Beck-Sickinger, A. G. High Molecular Weight PEGylation of Human Pancreatic Polypeptide at Position 22 Improves Stability and Reduces Food Intake in Mice. *Br. J. Pharmacol.* **2016**, *173*, 3208−3221.
(78) Frishman, W. H. Drug Therapy. Pindolol: A New β-Adrenoceptor Antagonist with Partial Agonist Activity. *N. Engl. J. Med.* **1983**, *308*, 940−944.
(79) Tenakin, T. P. Drug Antagonism: Orthosteric Drug Effects. In *Pharmacology in Drug Discovery and Development*, 2nd ed.; Academic Press, 2017; pp 65−100.
(80) Zhu, B. T. Mechanistic Explanation for the Unique Pharmacologic Properties of Receptor Partial Agonists. *Biomed. Pharmacother.* **2005**, *59*, 76−89.
(81) Moser, C.; Bernhardt, G.; Michel, J.; Schwarz, H.; Buschauer, A. Cloning and Functional Expression of the hNPY Y_5 Receptor in Human Endometrial Cancer (HEC-1B) Cells. *Can. J. Physiol. Pharmacol.* **2000**, *78*, 134−142.
(82) Cheng, Y.-C.; Prusoff, W. H. Relationship Between the Inhibition Constant (K_I) and the Concentration of Inhibitor Which Causes 50 Per Cent Inhibition (I_{50}) of an Enzymatic Reaction. *Biochem. Pharmacol.* **1973**, *22*, 3099−3108.
(83) Pegoli, A.; Wifling, D.; Gruber, C. G.; She, X.; Hübner, H.; Bernhardt, G.; Gmeiner, P.; Keller, M. Conjugation of Short Peptides to Dibenzodiazepinone-Type Muscarinic Acetylcholine Receptor Ligands Determines M_2R Selectivity. *J. Med. Chem.* **2019**, *62*, 5358−5369.
(84) Mach, H.; Middaugh, C. R.; Lewis, R. V. Statistical Determination of the Average Values of the Extinction Coefficients of Tryptophan and Tyrosine in Native Proteins. *Anal. Biochem.* **1992**, *200*, 74−80.
(85) Güntert, P. Automated NMR Structure Calculation with CYANA. In *Protein NMR Techniques*, Methods in Molecular Biology; Humana Press, 2004; Vol. *278*, pp 353−378.
(86) Gessmann, R.; Axford, D.; Bruckner, H.; Berg, A.; Petratos, K. A Natural, Single-Residue Substitution Yields a Less Active Peptaibiotic: The Structure of Bergofungin A at Atomic Resolution. *Acta Crystallogr. F Struct. Biol. Commun.* **2017**, *73*, 95−100. PDB DOI: https://doi.org/10.2210/pdb5MAS/pdb.
(87) Janes, R. W.; Hargittai, B.; Barany, G.; Maclean, E. J.; Teat, S. J. The High Resolution Crystal Structure of Alpha-Conotoxin Si to 0.75 Angstroms. 2003. PDB DOI: https://doi.org/10.2210/pdb1HJE/pdb
(88) Koradi, R.; Billeter, M.; Wüthrich, K. MOLMOL: A Program for Display and Analysis of Macromolecular Structures. *J. Mol. Graphics* **1996**, *14*, 51−55.
(89) Yang, Z.; Lasker, K.; Schneidman-Duhovny, D.; Webb, B.; Huang, C. C.; Pettersen, E. F.; Goddard, T. D.; Meng, E. C.; Sali, A.; Ferrin, T. E. UCSF Chimera, MODELLER, and IMP: An Integrated Modeling System. *J. Struct. Biol.* **2012**, *179*, 269−278.
(90) Pettersen, E. F.; Goddard, T. D.; Huang, C. C.; Meng, E. C.; Couch, G. S.; Croll, T. I.; Morris, J. H.; Ferrin, T. E. UCSF ChimeraX: Structure Visualization for Researchers, Educators, and Developers. *Protein Sci.* **2021**, *30*, 70−82.
(91) Trott, O.; Olson, A. J. AutoDock Vina: Improving the Speed and Accuracy of Docking with a New Scoring Function, Efficient Optimization, and Multithreading. *J. Comput. Chem.* **2010**, *31*, 455−461.
(92) Case, D. A.; Ben-Shalom, I. Y.; Brozell, S. R.; Cerutti, D. S.; Cheatham, T. E., III; Cruzeiro, V. W. D.; Darden, T. A.; Duke, R. E.; Ghoreishi, D.; Gilson, M. K.et al. *AMBER*; University of California: San Francisco, 2018; p 2018.
(93) Hornak, V.; Abel, R.; Okur, A.; Strockbine, B.; Roitberg, A.; Simmerling, C. Comparison of Multiple Amber Force Fields and Development of Improved Protein Backbone Parameters. *Proteins* **2006**, *65*, 712−725.
(94) Lindorff-Larsen, K.; Piana, S.; Palmo, K.; Maragakis, P.; Klepeis, J. L.; Dror, R. O.; Shaw, D. E. Improved Side-Chain Torsion Potentials for the Amber ff99SB Protein Force Field. *Proteins* **2010**, *78*, 1950−1958.
(95) Siu, S. W. I.; Vácha, R.; Jungwirth, P.; Böckmann, R. A. Biomolecular Simulations of Membranes: Physical Properties From Different Force Fields. *J. Chem. Phys.* **2008**, *128*, No. 125103.
(96) Lomize, M. A.; Lomize, A. L.; Pogozheva, I. D.; Mosberg, H. I. OPM: Orientations of Proteins in Membranes Database. *Bioinformatics* **2006**, *22*, 623−625.
(97) Wolf, M. G.; Hoefling, M.; Aponte-Santamaría, C.; Grubmüller, H.; Groenhof, G. g_membed: Efficient Insertion of a Membrane Protein into an Equilibrated Lipid Bilayer with Minimal Perturbation. *J. Comput. Chem.* **2010**, *31*, 2169−2174.
(98) Darden, T.; York, D.; Pedersen, L. Particle Mesh Ewald: An N·log(N) Method for Ewald Sums in Large Systems. *J. Chem. Phys.* **1993**, *98*, 10089−10092.
(99) Berendsen, H. J. C.; Grigera, J. R.; Straatsma, T. P. The Missing Term in Effective Pair Potentials. *J. Phys. Chem. A* **1987**, *91*, 6269−6271.
(100) Abraham, M. J.; Murtola, T.; Schulz, R.; Páll, S.; Smith, J. C.; Hess, B.; Lindahl, E. GROMACS: High Performance Molecular Simulations Through Multi-Level Parallelism from Laptops to Supercomputers. *SoftwareX* **2015**, *1-2*, 19−25.
(101) Hunter, J. D. Matplotlib: A 2D Graphics Environment. *Comput. Sci. Eng.* **2007**, *9*, 90−95.

Downloaded from pubs.acs.org/jmcmar/article-pdf/66/14/9642/4587513/jm3c00363.pdf by FREIE UNIV BERLIN user on 14 November 2026